Modeling of Adsorption of Molecules in Pristine and Defective UiO-66

by

Priyanka Bholanath Shukla

Bachelor of Technology in Chemical Engineering, Ahmedabad University, 2015

Master of Science in Chemical Engineering, University of Pittsburgh, 2019

Submitted to the Graduate Faculty of

the Swanson School of Engineering in partial fulfillment

of the requirements for the degree of

Master of Science

University of Pittsburgh

2021

UNIVERSITY OF PITTSBURGH

SWANSON SCHOOL OF ENGINEERING

This thesis was presented

by

Priyanka Bholanath Shukla

It was defended on

April 4, 2021

and approved by

J. Karl Johnson, Ph.D., William Kepler Whiteford Professor,Department of Chemical and Petroleum Engineering

Christopher E. Wilmer, Ph.D., Department of Chemical and Petroleum Engineering

Nathaniel L. Rosi, Ph.D., Department of Chemical and Petroleum Engineering

Thesis Advisor: J. Karl Johnson, Ph.D., William Kepler Whiteford Professor,Department of Chemical and Petroleum Engineering

Modeling of Adsorption of Molecules in Pristine and Defective UiO-66

Priyanka Bholanath Shukla, M.S.

University of Pittsburgh, 2021

Metal-organic frameworks are nanoporous materials that are used for various applications such as gas adsorption, storage, and separations. Our work focuses mainly on the UiO family of Zr-based MOFs, which may be used to capture and destroy chemical warfare agents (CWA) and their simulants. We have studied the adsorption of molecules such as nitrogen, isopropanol, and acetone in UiO-66 with different framework and molecule potentials in order to understand the basic interactions and adsorption mechanism.

The fully coordinated dense structure of UiO-66 has very small pore windows that limit access of larger molecules and thus decreases the adsorption capacity for CWAs. Thus, we have created missing linker defects in Pristine UiO-66 in order to increase accessibility to the pores. Defects may be created experimentally by adding modulators such as acetic acid, formic acid, hydrochloric acid, and other solvents while synthesizing the UiO-66 material where they compete with the organic linkers to form bonds with the Zr_6 metal clusters. We have studied the adsorption of molecules in defective UiO-66 with different capping groups such as hydroxide, formate, and acetate and increasing the level of defects. We have studied 4%, 8%, 17%, and 33% missing linker defects. We observe that the saturation uptake increases with the increase in the defect level.

The modeling was done by holding the framework structure rigid in-order to increase the computational efficiency. However, the intrinsic framework flexibility may have a significant impact on the adsorption. To further explore this phenomenon, we have studied the impact of intrinsic framework flexibility on the adsorption of acetone and nitrogen in pristine UiO-66. The modeling was done by performing GCMC simulations on structures generated from NVT-MD snapshots of the empty and finite loaded UiO-66 framework. The results show that introducing framework flexibility increases the adsorption of acetone for both the empty framework and finite loading acetone framework but does not accommodate more nitrogen molecules. This suggests that accurate isotherms require NVT-MD simulations with finite

loading of the desired molecule in the framework, followed by modeling of the adsorption isotherm.

Table of Contents

List of Tables

List of Figures

1.0 Introduction

Metal Organic Frameworks (MOFs) are nanoporous materials composed of inorganic nodes connected by organic linkers. The MOFs find many applications in fields[1, 2] such as catalysis, gas adsorption[3, 4, 5, 6, 7], storage and separation[8, 9, 10, 11], drug delivery and many more due to the porous structure and large surface area. The organic linkers can also be tuned by orienting the size and functional group to provide the required practicality to the framework [12]. The gas adsorption mechanism is driven by the interactions of organic linker-guest molecule present in the MOFs. The modifications to the linker affects the MOF-adsorbate interactions and enhances the selectivity for specific adsorbates. Of all the other MOFs, Zr derived metal organic frameworks have become popular as compared to other MOFs due to their high thermal and mechanical stability [13, 14, 15, 16, 17, 18, 19, 20, 21]. These materials are also stable in chemical solvents and show high resistance to shear stress [22]. Thus, Zr-derived MOFs has gained application in several science fields.

Our work focuses mainly on the UiO family of Zr-based MOFs, which are used to capture and destroy chemical warfare agents (CWAs) and their simulants [3, 23, 24, 25, 26, 27]. We have performed modeling of adsorption of polar and non-polar molecules such as nitrogen, isopropanol and acetone in UiO-66. UiO-66 belongs to UiO family and was found in the University of Oslo [13]. It consists of metal clusters of $[Zr_6O_4(OH)_4]$ and 1,4-benzodicarboxylic acid (BDC) organic linkers. Each Zr_6 metal cluster center consists of 4 μ_3-OH and 4 μ_3-O groups and is connected to 12 BDC linkers, with each linker shared between the two Zr_6 metal clusters as shown in Figure 1. Thus the zirconium atoms in the metal cluster are fully coordinated. The strong bonding between Zr and carboxylate O atom is due to the high charge density and bond polarization that makes the structure thermally,chemically and mechanically stable [28]. It is also stable in water, organic solvents and acids [29, 30, 31]. The study of adsorption has widely been done in dehydroxylated UiO-66 which is achieved by heating or keeping it under high temperature in vacuum [32, 33]. The dehydroxylation of the framework eliminates the μ_3-OH groups. In this work, we have studied the adsorption of molecules in hydroxylated UiO-66 structure. However, the fully coordinated structure limits

the access of the pores for adsorption and thus decreases the adsorption capacity of large molecules [34]. Recent studies have shown that the synthesized UiO-66 material contains some amount of missing linker defects, by thermogravimetric analysis (TGA)[32]. The UiO-66 structure can bear the missing linker defect as compared to the other MOFs coordinated by 4-,5- or 6- organic linkers where the pores collapse and forms the boundary type defect instead the missing linker defect [35]. Some studies have reported that the UiO-66 pore structure can be retained even after removing up to 4.3 linkers per Zr metal cluster [36].

Two types of defect may be present in the UiO-66 structure - missing linker and missing zirconium metal cluster defects. These defects modify the framework properties such as porosity, surface area, catalytic activities, and other physical and chemical properties. They also change the adsorption chemistry [37, 38, 39, 40, 41] and enhance the performance in fields such as separation, catalysis, sorption and many more[35]. Snurr et al. [42] in the study of impact of missing linker defects on the adsorption of water in UiO-66 has reported that the defect sites in the MOF makes the material more hydrophilic and shows higher water adsorption.

Since each linker is shared between the two Zr metal nodes in UiO-66, removing a linker causes two defect centers forming an unsaturated Zr sites. To create a missing linker defect, modulators such as formic acid, hydrochloric acid, acetic acid, benzoic acid or any-other acids are added besides the organic linkers. These modulators compete with the BDC linkers to form bonds with the Zr_6 metal clusters. They form bonds with the Zr_6 metal center and remain attach to it producing the missing linker defects. This also implies that adding larger amounts of modulators would lead to more missing linker defects in the framework. The modulators control the density and chemical functionality of the frameworks. The created defects in the framework increase the BET surface area proportionally by increasing the porosity. These defects allow the adsorption of larger molecules which was inhibited in Pristine UiO-66 due a pore size of 6 Å as reported by Jiao et al [43]. The paper reported that the adsorption increased with an increase in the BET surface area (from 1179 to 1808 m^2/g)for SO_2 with pore size of 4.1 Å. For molecule size greater than 6 Å, the adsorption improved due to the creation of supermicropores by the missing linker defects. This was shown in one of the studies where the adsorption capacity of toluene increased by 1.8 times than

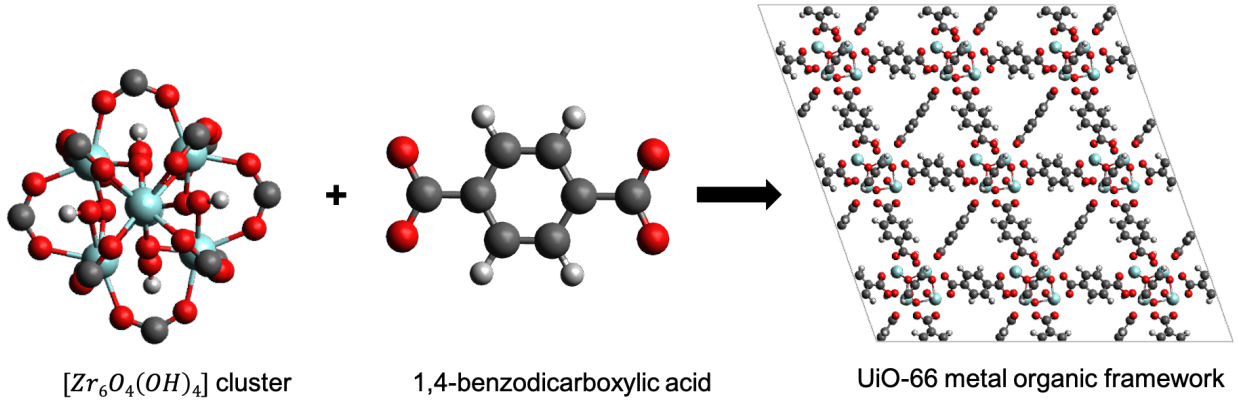

Figure 1: 3x3x3 super cell of UiO-66 MOF. Each unit cell consists of two tetrahedral and one octahedral pore. The framework consists of zirconium metal cluster and BDC organic linkers. Carbon, oxygen, hydrogen and zirconium atoms are shown in gray, red, white and cyan respectively.

in Pristine UiO-66 [44]. Moreover, these missing linker/cluster defects allow mass transfer diffusion especially of large pore size molecules. This was evident from the study of free energy of uranyl ion diffusion by Yuan et al. [45], where the free energy was 31 kcal/mol in Pristine UiO-66 and 17.4 kcal/mol in Defective UiO-66. The type of modulator determines the linker vacancies in UiO-66. Modulators such as TFA and formate are dominant modulators than acetic acid due to the lower pK_a (0.23) value than of acetic acid (4.76) and generate highly defective UiO-66 structures. These defects are created due to competitive binding of the BDC linkers (pK_a = 4.82) and modulators with the metal cluster. Adding TFA creates more deprotonated modulators than deprotonated BDC linkers that compete to bind with the carboxylate sites of the metal cluster giving more defective UiO-66 structure [46]. Whereas adding acetic acid doesn't compete much with the BDC linkers and creates less defective structures. In this study, we have emphasized on the adsorption of molecules in defective UiO-66 with different capping groups such as hydroxide, formate, and acetate and increasing the level of defects. We have studied the adsorption of molecules in 4%, 8%, 17% and 33% missing linker defects. These capping groups act as charge neutrality for the

unsaturated metal sites created by the missing linker. Lastly, we have studied the impact of intrinsic framework flexibility on the adsorption of acetone and nitrogen in Pristine UiO-66. The modeling was done by performing GCMC simulations on structures generated from canonical ensemble (NVT) molecular dynamics snapshots of the empty UiO-66 framework and also with a loading of 7 acetone per unit cell of UiO-66. The results show that the finite loading has a nontrivial impact on the adsorption ability of the framework.

1.1 Methods

The non-bonded interactions are defined by the Lennard Jones 12-6 potential which is a pairwise-additive interaction as defined in equation (1-1). σ_{ij} , ϵ_{ij} and r_{ij} are Lennard-Jones size, depth and the separation, respectively for all pair of atoms i and j, where i is for framework atoms and j is for the guest molecule. The Lennard Jones parameters are calculated with the Lorentz-Berthelot combining rules for the unlike pair of atoms as described in equation (1-2)-(1-3)

.

$$U(r_{ij}) = 4\epsilon_{ij}\left[\left(\frac{\sigma_{ij}}{r_{ij}}\right)^{12} - \left(\frac{\sigma_{ij}}{r_{ij}}\right)^{6}\right] \tag{1-1}$$

$$\sigma_{ij} = \left(\sigma_{ii} + \sigma_{jj}\right)/2 \tag{1-2}$$

$$\epsilon_{ij} = \sqrt{\epsilon_{ii}\epsilon_{jj}} \tag{1-3}$$

For TraPPE-United Atom (UA) model, the bond lengths are kept fixed for the molecules. Nevertheless, the change in energy due to bond stretch and contract can be defined by Harmonic bonding potential as described in equation (1-4)

$$U = \frac{1}{2}p_0\left(r - p_1\right)^2 \tag{1-4}$$

The bond angle bending is measured by harmonic bending as described in equation (1-5) where θ_{ijk}, p_1 and p_0 are the measured angle, equilibrium bend angle and force constant,

Table 1: Modified UFF Lennard Jones parameters for UiO-66 framework atoms to account for hydrogen bonding

Atom	ϵ/k_b(K)	σ(Å)
Zr	34.722	2.783
O	30.193	3.118
C	52.838	3.431
H	22.142	2.571
mu3O	93.00	3.020
mu3H	0.000	0.000

respectively.

$$U_{bend} = \frac{1}{2} p_0 \left(\theta_{ijk} - p_1\right) \tag{1-5}$$

The intramolecular rotations are defined by Fourier expansion torsional potentials for atoms separated by three bonds as shown in equation (1-6) where c_0, c_1, c_2 and c_3 are the Fourier coefficients.

$$U_{tors} = c_0 + c_1 \left[1 + \cos\left(\theta\right)\right] + c_2 \left[1 - \cos\left(2\theta\right)\right] + c_3 \left[1 + \cos\left(3\theta\right)\right] \tag{1-6}$$

We have used Universal Force field (UFF) and DREIDING to describe the Lennard Jones parameters of the framework atoms as described in Table 1 and 2. The LJ parameters of μ_3-OH oxygen and hydrogen in UFF were changed to TraPPE isopropanol O and H parameters to capture the hydrogen bonding phenomenon. The bonded and non-bonded parameters for nitrogen, acetone and isopropanol are described in Table 3

We have created 4%, 8%, 17% and 33% missing linker defects in pristine UiO-66. All the structures were generated and relaxed by Xin Wei, Graduate Student at the University of Pittsburgh. The pristine primitive cell consists of one SBU unit (comprised of 6 Zr atoms, 4 μ_3-OH and 4 μ_3-O groups) and 6 BDC linkers. To create 4% missing linker defect, a super cell of 2x2x1 (contained 4 SBUs and 24 linkers) was generated and a linker was removed as

Table 2: DREIDING Lennard Jones parameters for UiO-66 framework atoms

Atom	ϵ/k_b(K)	σ(Å)
Zr	34.722	2.783
O	48.159	3.033
C	47.859	3.473
H	7.6497	2.846

shown in Figure 4. 8% defective UiO-66 was generated by developing a supercell of 2x1x1 (contained 2 SBUs and 12 linkers) from a formula unit cell and removing a linker (Figure 3). 17% defect level was generated by removing a linker from a formula unit (Figure 2). Similarly, two linkers were removed from the primitive cell to create 33% defect in UiO-66 (Figure 5). The generated defective cell structures were then relaxed with density functional theory and atomic charge densities were computed from DDEC6. When a linker is removed it creates unsaturated Zr metal sites, opening four metal sites; two sites each on both the metal clusters. To balance the charges created by removing the linkers, we add several charge balancing groups such as hydroxyl, formate and acetate groups. These capping groups are added on each side of the open metal cluster to saturate it. Studies have shown, that there are two ways of adding OH groups on each side of the removed missing linker. The two ways are adding OH groups either on trans or cis form, of which trans configuration gives lowest energy structure, explained by the electrostatic and steric hinderance effects reported by Bristow et al. [47]. There is only one way to add formate and acetate groups for the removed linker as shown in Figure 6.

Table 3: Bonded and Non-bonded parameters for TraPPE-UA isopropanol, nitrogen and acetone

bond-stretch	r_0 (Å)
CH_x-CH_y	1.540
CH_x-OH	1.540
O–H	1.540
CH_x-C	1.520
C=O	1.229

bend	θ (degree)	p_0(K)
$CH_x-(CH)-CH_y$	112.0	62500
$CH_x-(CH_y)-O$	109.5	50400
$CH_x-C(=O)-CH_y$	117.2	62500
$CH_x-C=O$	121.4	62500
$CH_x-(O)-H$	108.5	55400

Torsion	c_o(K)	c_1(K)	c_2(K)	c_3(K)
$CH_x-(CH)-(O)-H$	215.96	197.33	31.46	-173.92

Atom	ϵ/k_b(K)	σ(Å)	q
N_N_2	36.0	3.310	-0.482
N_com	0	0	+0.964
$(CH_x)_2-(CH)-OH$	10	4.330	+0.265
$CH_x-(O)-H$	93	3.020	-0.700
$(CH_3)-CH_x$	98	3.75	0
C(sp^2)	40.0	3.820	+0.424
O(sp^2)	79.0	3.050	-0.424
CH_3(sp^3)	98.0	3.750	0

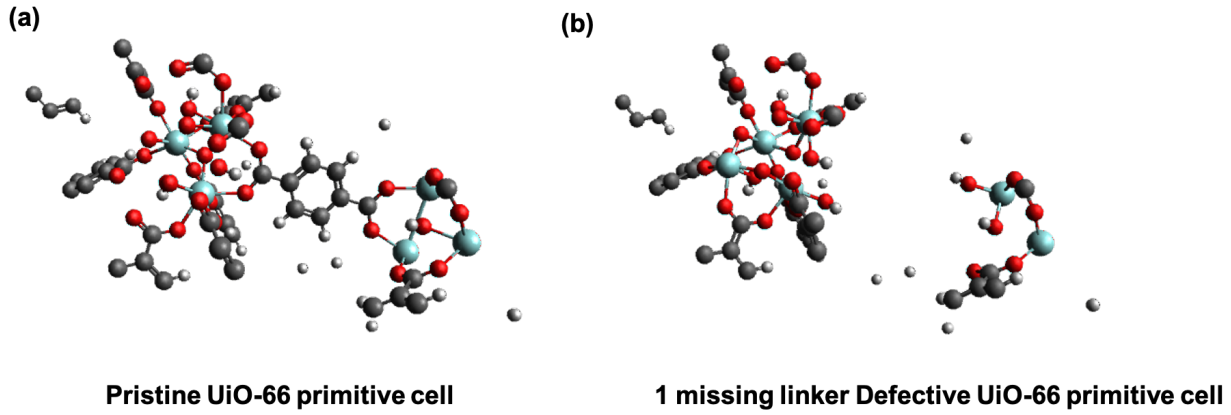

Figure 2: (a) Pristine UiO-66 framework in a primitive cell. (b) 1 missing linker per primitive cell creating 17% defect level in UiO-66. The defective UiO-66 is capped with two hydroxide groups for one missing linker. Studies have been done using other capping groups also.

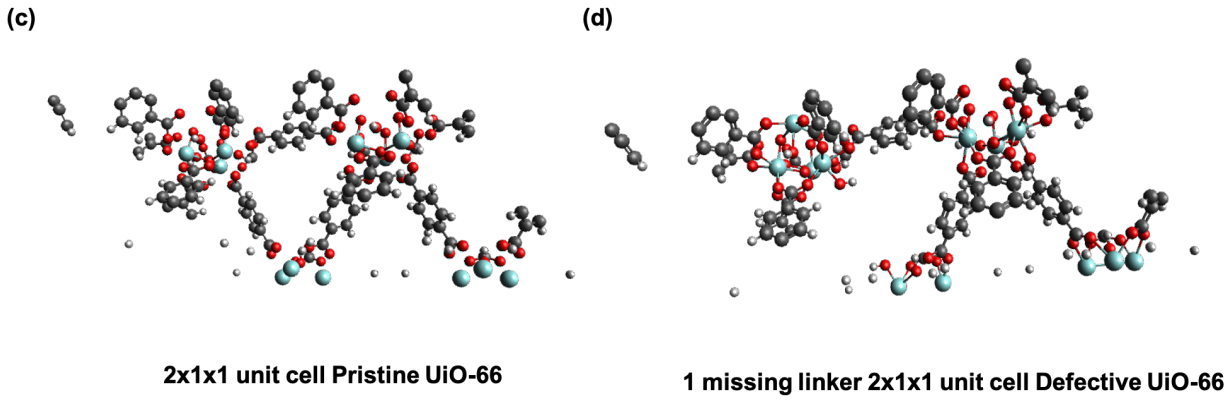

Figure 3: (c) Pristine UiO-66 framework in a 2x1x1 super-cell. (d) 1 missing linker per 2x1x1 unit cell creating 8% defect level in UiO-66. The defective UiO-66 is capped with two hydroxide groups for one missing linker. Studies have been done using other capping groups also.

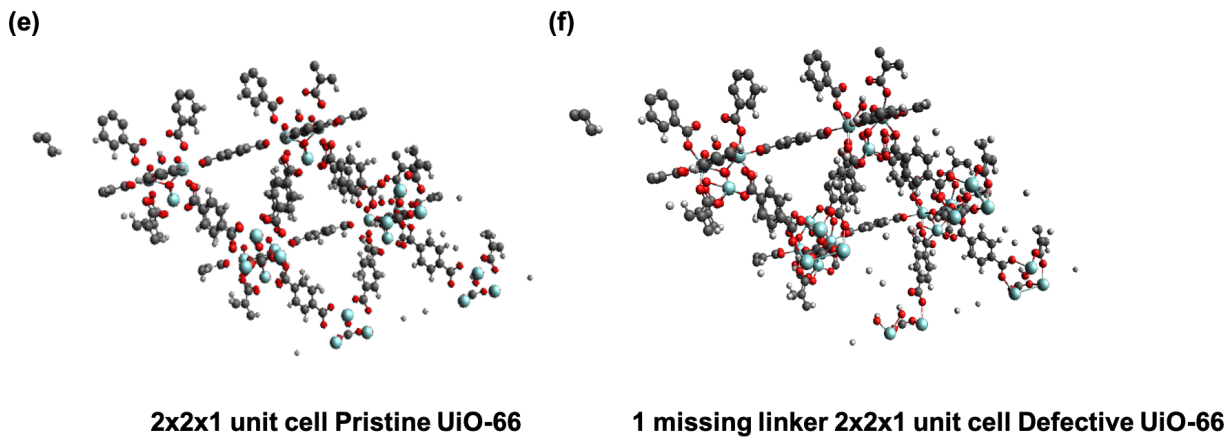

Figure 4: (e) Pristine UiO-66 framework in a 2x2x1 super-cell. (f) 1 missing linker per 2x2x1 unit cell creating 4% defect level in UiO-66. The defective UiO-66 is capped with two hydroxide groups for one missing linker. Studies have been done using other capping groups also.

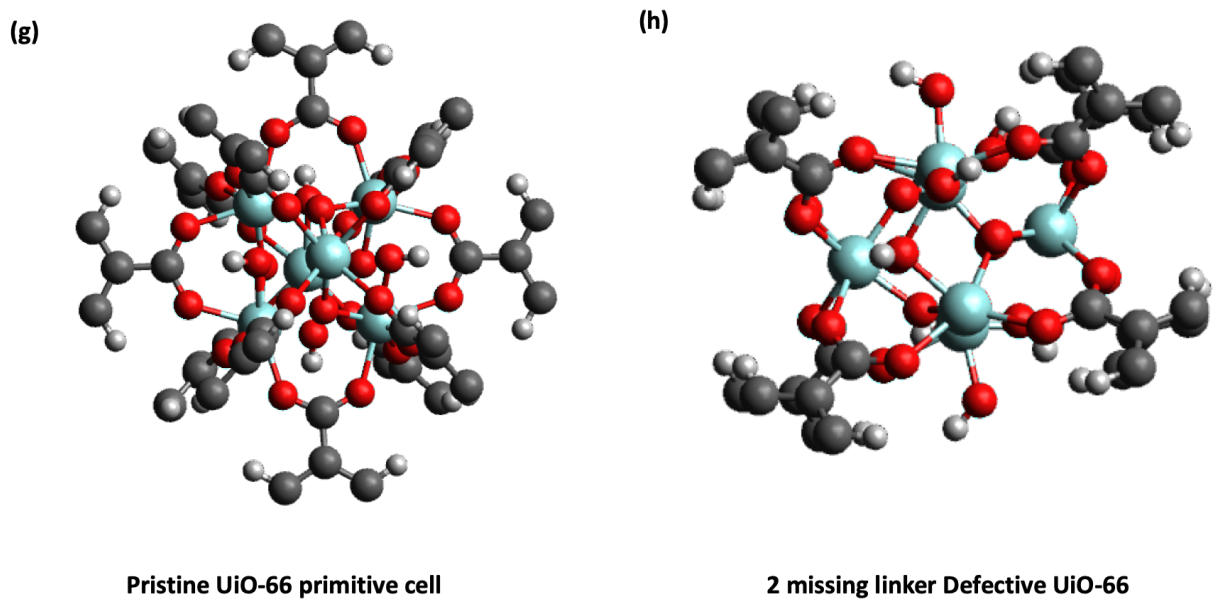

Figure 5: (g) Pristine UiO-66 framework in a primitive cell. (h) 2 missing linkers per primitive cell creating 33% defect level in UiO-66. The defective UiO-66 is capped with four hydroxide groups for two missing linkers. Studies have been done using other capping groups also.

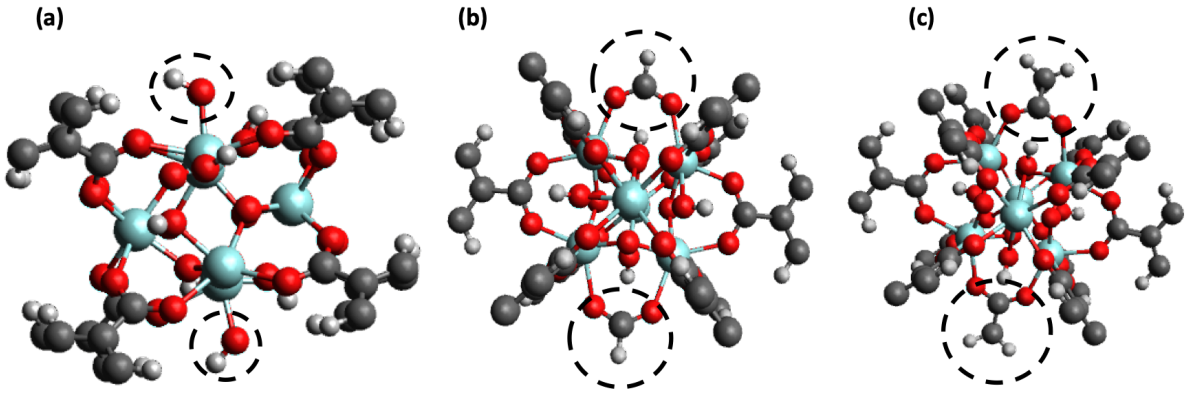

Figure 6: Defective UiO-66 unit cell capped with modulators: (a) -OH groups (b) formate groups (c) acetate groups. The capping groups are enclosed in a dashed circle. Two capping groups are bonded with the Zr_6 metal cluster for each missing linkers.

2.0 Adsorption of Nitrogen in Pristine and Defective UiO-66

2.1 Introduction

In this project, we have studied two models of nitrogen molecule to perform the adsorption of nitrogen molecules in UiO-66. The nitrogen potentials are nonpolarizable all-atom transferable potential for phase equilibria (TraPPE) forcefield and potential with high accuracy, speed, and transferability (PHAST) forcefield. The TraPPE N_2 model uses Lennard-Jonnes potentials for the overlap and dispersive interactions and simple point charges for the first order induction and electrostatic interactions. It is a three site model with two Lennard Jones sites separated by the bond length of 1.10 Å. These Lennard Jones sites have point charges of -0.482 e. The center of mass (COM) of the nitrogen molecule has a point charge of +0.964 e to maintain the charge neutrality. The schematic diagram of N_2-TraPPE model is shown in Figure 7. PHAST forcefield neglects the effect of polarization for making the potential suitable for molecular dynamics and Monte Carlo simulations. It is a transferable potential and includes all essential potential energy interactions for describing complex systems . The potentials includes contribution to the many-body polarization, electrostatic and the electronic repulsion/dispersion as shown in equation (2-1).

$$U = U_{pol} + U_{es} + U_{rd} \tag{2-1}$$

N2-PHAST is a five site nitrogen model. The two sites are atom-centered and are the only mass containing sites. Third site is at the center of the nitrogen molecule. The remaining two sites are at the extremes of the molecules. The positions of these two sites were constrained to the z-axis, ensuring the equal displacement of the COM as shown in Figure 8.

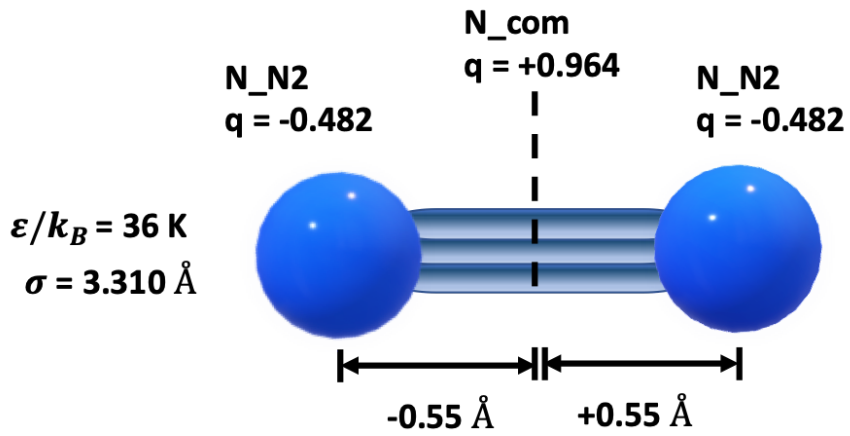

Figure 7: Nitrogen TraPPE force field schematic diagram. It is a three site model with two LJ sites and a compensating charge at the COM of the N_2 molecule.

2.2 Calculation Methods

Grand Canonical Monte Carlo (GCMC) simulations were performed to simulate N_2 adsorption isotherm at 77 K in pristine UiO-66, using the RASPA software package [48].The simulations assumed rigid framework to calculate the adsorption isotherms as done commonly for large adsorbent structures[49]. The Peng-Robinson equation of state was used to calculate the fugacity, which was used in the simulations. The ideal gas rosenbluth weight was calculated to be 1.0 for nitrogen. Each pressure in the isotherm used 20,000 equilibration cycles and 20,000 production cycles to compute the ensemble averages. In each Monte Carlo cycle, an average of N moves were performed, where N is the number of adsorbate molecules in the system. A 3x3x3 super cell of UiO-66 was used. The primitive cell of UiO-66 comprised of 114 framework atoms, thus 3048 framework atoms in the 3x3x3 super cell. Translational, rotational, reinsertion and swap moves were performed with the relative probabilities in the ratio of 1:1:1:2. A cut off of 14 Åwith standard tail-corrections was

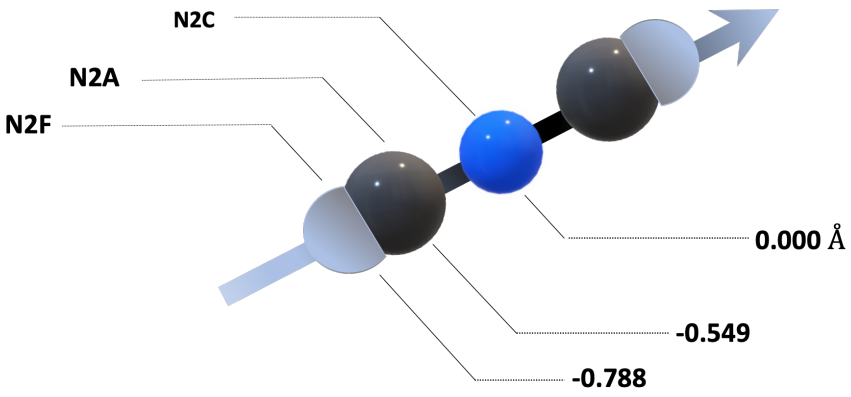

Figure 8: N_2-PHAST five site schematic diagram with three different sites as follows: White: N2F, Black: N2A and Blue: N2C. The COM of the model resides at N2C. The Lennard Jones sites are N2C and N2A. The potential parameters are in Table 4. The arrow represents the z-axis.

used to approximate the van der Waals interactions beyond the cut-off [50].Lorentz-Berthlot combining rules were used for the unlike interactions. The Helium void fraction was calculated to be 0.47 by probing the helium molecules in the framework at room temperature. Ewald summation [51] was used for calculating the coulombic interactions of both adsorbate-adsorbate and adsorbent-adsorbate interactions. Atomic charges for the UiO-66 framework atoms were computed using Density-derived electrostatic and chemical charges (DDEC6) [52, 53, 54, 55].The Lennard Jones paramaters were taken from the UFF[56] and DREIDING forcefields [57] except for Zr which was taken from UFF for all the UiO-66 framework atoms.

Table 4: N_2-PHAST Potential parameters with sites: N2A, N2C and N2F

site	Q (e)	R (Å)	ϵ (K)	σ (Å)
N2C	1.0474	0.000	25.6443	3.4442
N2F	0.000	± 0.788	15.5320	3.0729
N2A	-0.5237	± 0.549	0.000	0.000

2.3 Result and Discussion

2.3.1 Impact of Framework and Fluid Potentials on the Adsorption of Nitrogen in Pristine UiO-66

Figure 9 shows the plot of N_2 adsorption isotherm at 77 K via GCMC simulations. Our simulations were compared with the literature data to validate its accuracy. The impact of the fluid potential on the adsorption was examined by two N_2 models - TraPPE and N_2-PHAST. The impact of framework potential was studied by UFF and DREIDING forcefields. We observe that both the framework and N_2 potentials gave the same amount of N_2 molecules adsorbed at the saturation loading. N_2-PHAST fluid potential gave approximately similar results to TraPPE N_2 and UFF framework potentials in low pressure regime. The intermediate part of the N_2-PHAST model was in between TraPPE-UFF and TraPPE-DREIDING forcefields. The simulation isotherm shapes and saturation loading for N_2 in pristine UiO-66 are in good agreement with the experimental results published by Katz et al. (Figure S10) [12] and Shearer et al. (Figure S27) [46].

2.3.2 Adsorption of Nitrogen in Defective UiO-66 for Different Capping Groups

We have also studied the impact of different capping groups on the adsorption of N_2 at 77K in Defective UiO-66 via GCMC simulation. Figure 10 shows the adsorption isotherm of N_2 in OH capped (2 OH groups for each missing linker) Defective UiO-66 in different

defect levels. At low pressure regime, the N_2 uptake decreases with the increase in the level of defects. This is because the lower pressure regime of the adsorption isotherm is governed by the surface area which is highest for Pristine UiO-66 followed by 4%, 8%, 17% and 33% defect levels. More availability of the surface atoms allows more number of N_2 molecules to interact with the available framework atoms which increases the adsorption loading. The adsorption loading of Pristine and 4% defective UiO-66 are similar at low pressure. This is because as we remove the linker to create a defect, the surface area of the framework decreases but the framework mass increases due to the increase in molecules per unit cell. Thus these two counter phenomena nullify the effect and give us similar adsorption at lower loading. After the cross-over at 1 Pa, the high pressure regime is dominated by the free volume of the framework. Thus the adsorption increases with the increase in the level of defects. Figure 11 shows the adsorption isotherm of N_2 in several level of defects in UiO-66 capped with the formate group. At low pressure regime, the adsorption decreases with the increase in the level of defects since the number of surface atoms decreases for the nitrogen atoms to interact with. For P>1 Pa, i.e., at higher pressure part of the isotherm, the order is reversed because the adsorption is governed by the available free volume which is highest for 33% defect level followed by 17%, 8%, 4% and Pristine UiO-66. Note that the adsorption is higher for formate capping groups than OH capping group in the low pressure regime because the formate group is bigger than OH group which leads to more number of available surface atoms. We have also compared the impact of OH, formate and acetate capping groups on the adsorption of nitrogen in 17% defective UiO-66 as shown in Figure 13. The adsorption is highest for Pristine followed by acetate, formate and then OH capped Defective UiO-66 in low pressure regime. At high pressure regime, the order is exactly reversed because of the free volume argument. We have also compared the adsorption isotherm of the synthesized sample of UiO-66 with the simulated isotherms of Pristine UiO-66 and Defective UiO-66 capped with formate groups as shown in Figure 13. The synthesized UiO-66 depicts type I adsorption isotherm with a BET surface area of 1100 m^2g^{-1} which is consistent with the result of Shearer et al. [58] for minimum level of defects in UiO-66. The higher pressure part of the experimental adsorption isotherm was similar to 8% defect level capped with formate group. However, all of our simulated isotherms in Figure 13 rises steeply than

increasing gradually as shown by the experiments. This could be due to the assumption of the uniform pores and perfectly crystalline structure of the framework in our simulations while the synthesized UiO-66 has complex pore structure. At saturation pressure,the N_2 uptake deviates and increases indicating the presence of mesopores in the prepared UiO-66 sample. The simulated adsorption isotherms do not show such increase at the saturation pressure because of the uniform pore structure.

2.4 Conclusion

We have modeled the adsorption of N_2 at 77 K in pristine UiO-66 with different N_2 models and framework potentials. The modeled simulations are in good agreement with the experiments and follow Langmuir Type I isotherm. Moving forward we have studied the impact of different capping groups such as hydroxide, formate and acetate groups on the adsorption of N_2 in Defective UiO-66. We have studied missing linker defects in this work with 4%, 8%, 17% and 33% defect levels. For all type of defects, the low pressure regime is dominated by available surface are and so the N_2 is highest for Pristine, followed by increasing level of defects. However, the high pressure regime is governed by free volume in the framework and thus the order is exactly flipped. We have also shown the impact of different capping groups on the adsorption of N_2 at 17% defect level. The argument for the behaviour is governed by available surface area and pore volume at low pressure and high pressure regime respectively. Thus, at low pressure, the loading is highest for pristine, followed by acetate, then formate and lastly hydroxide group. The high pressure regime is dominated by the free volume, so the order gets flipped.

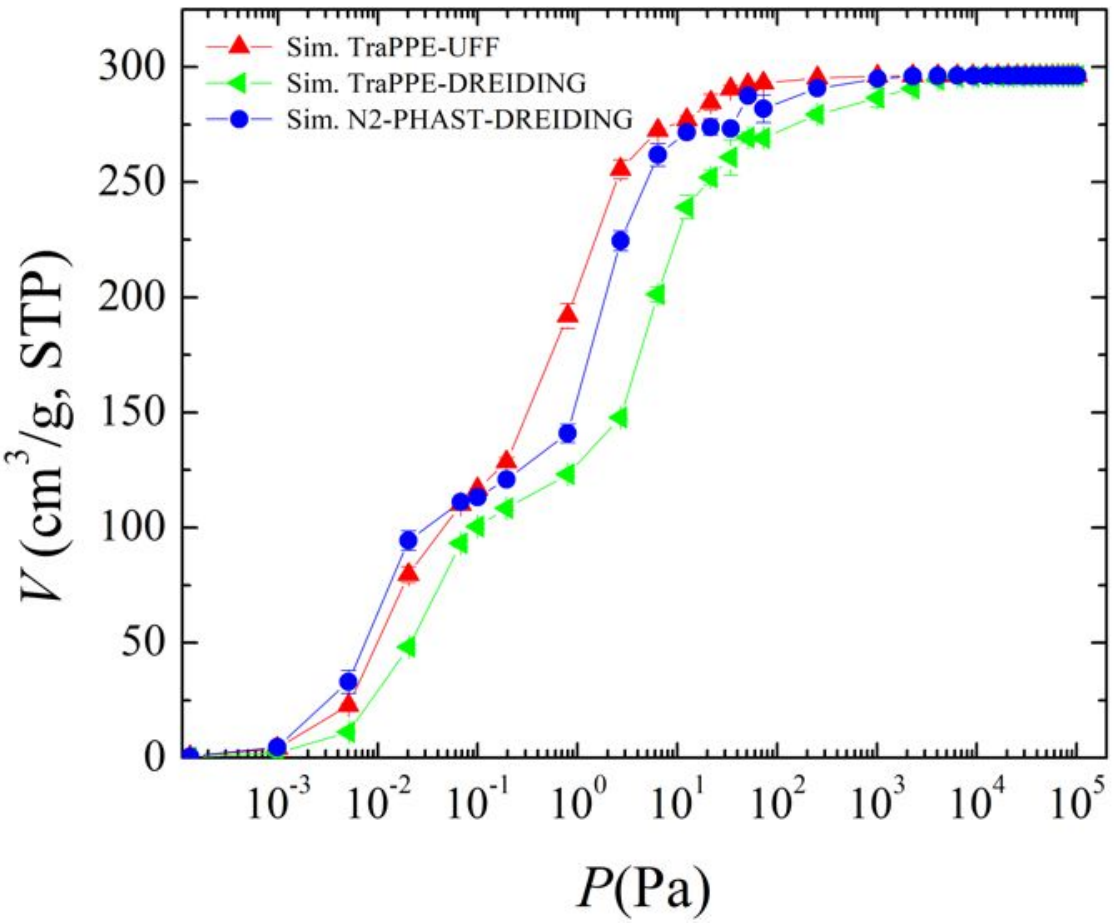

Figure 9: Adsorption isotherm of nitrogen at 77 K via GCMC simulations for various molecule (TraPPE (red up triangles) and N_2-PHAST (blue circles) and framework (UFF and DREIDING) potentials)

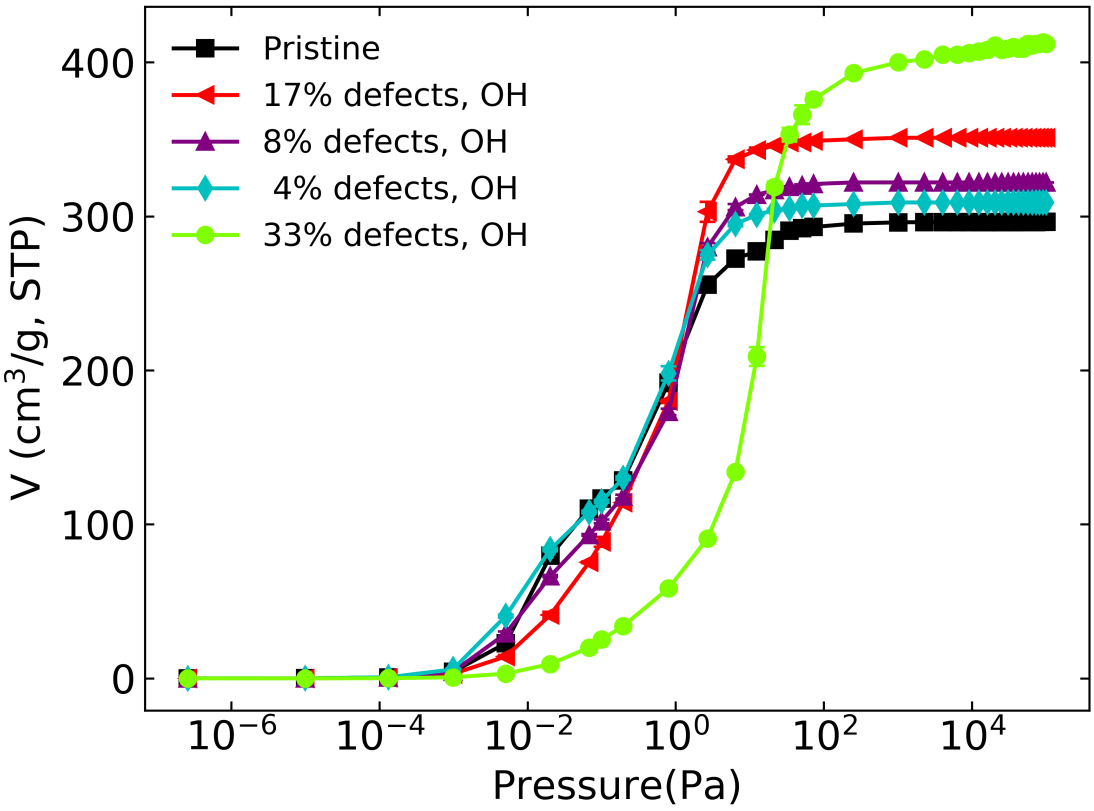

Figure 10: Adsorption isotherm of nitrogen at 77 K via GCMC simulations with several level of missing linker defects in UiO-66 and added OH capping group

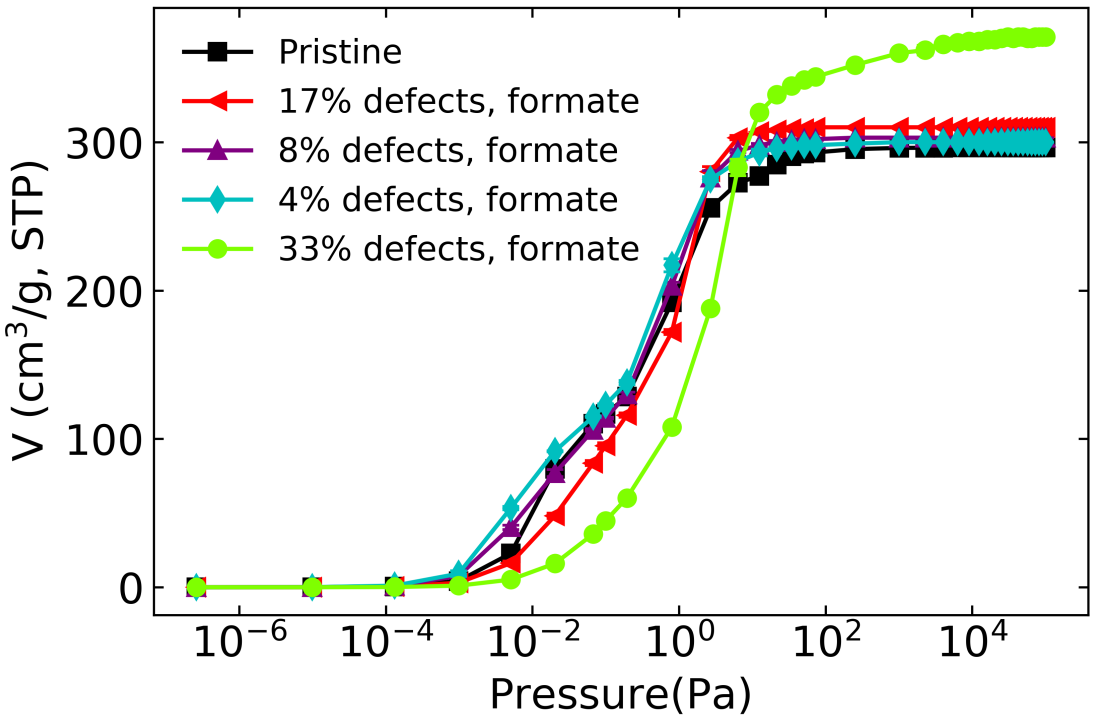

Figure 11: Adsorption isotherm of nitrogen at 77 K via GCMC simulations with several level of missing linker defects in UiO-66 and formate capping group

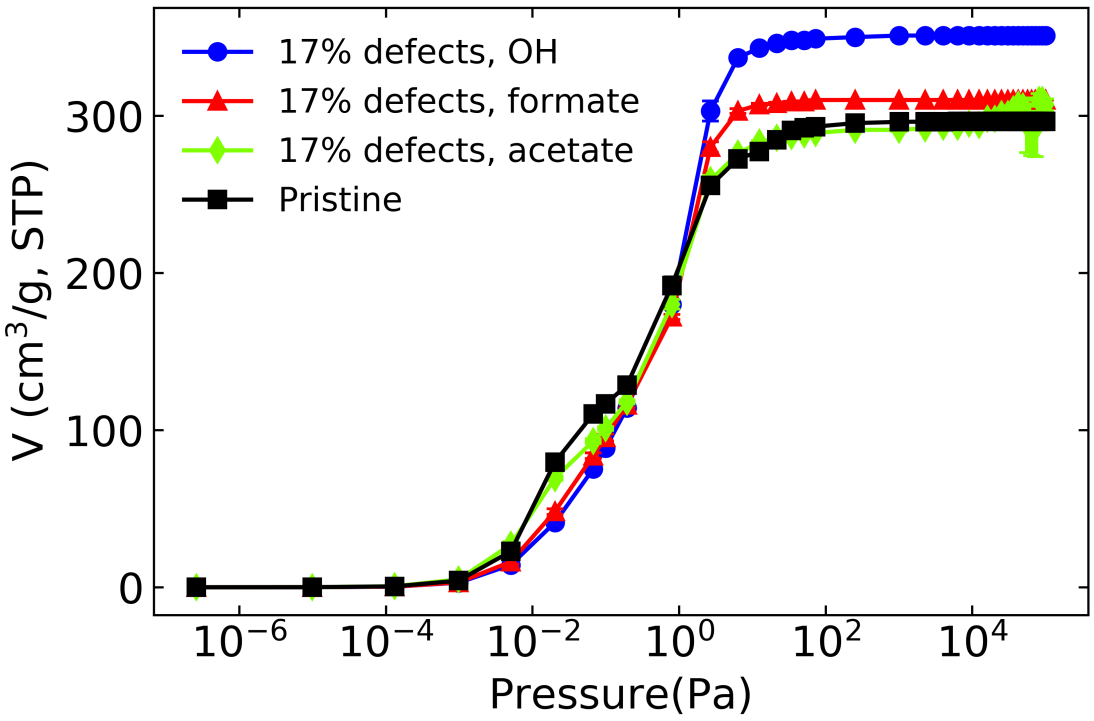

Figure 12: Adsorption isotherm of nitrogen at 77 K via GCMC simulations for Pristine and 17% defective UiO-66 capped with OH, acetate and formate groups

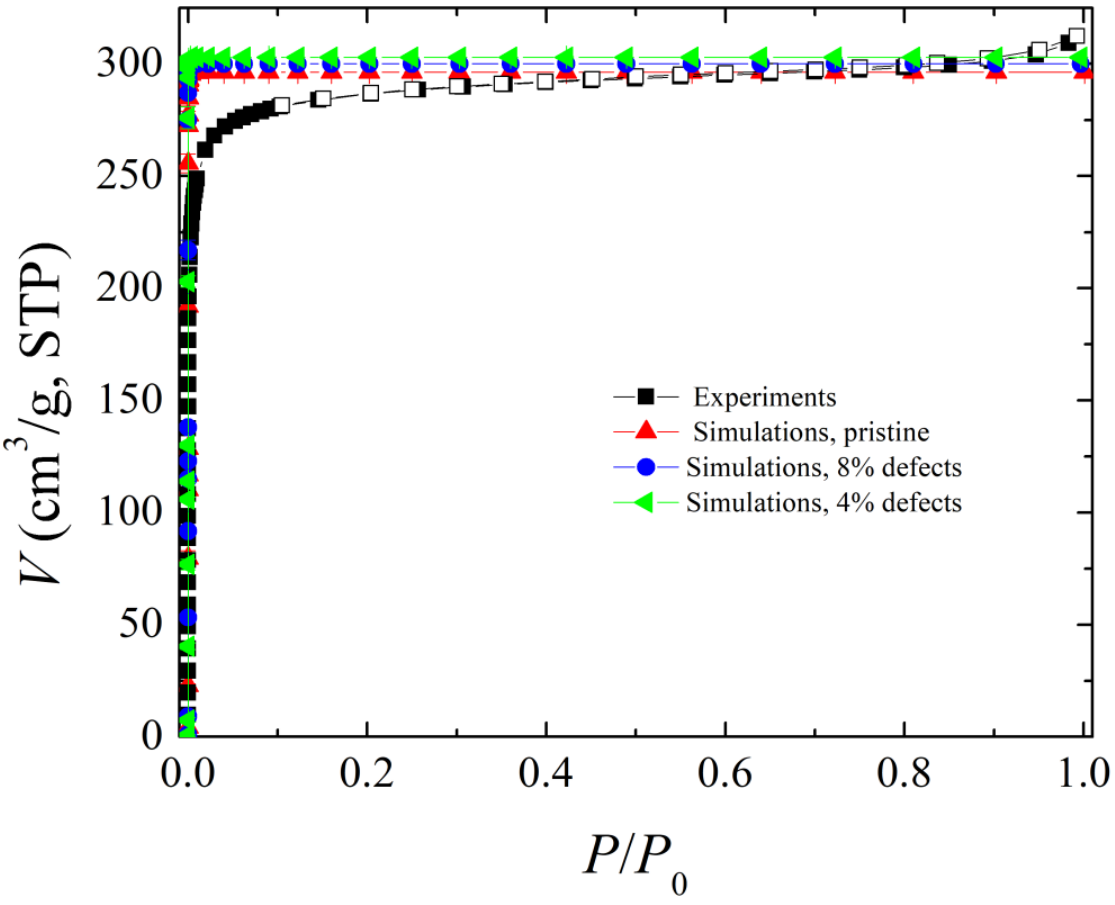

Figure 13: Adsorption isotherm of nitrogen at 77 K via GCMC simulations for pristine,4% and 8% formate capped defect levels and its comparison with the Experiments

3.0 Adsorption of Isopropanol in Pristine and Defective UiO-66

3.1 Introduction

In this project, we have studied three different isopropanol (IPA) models - TraPPE, SKS and OPLS-AA and two different UiO-66 framework potentials - DREIDING and UFF for modeling the adsorption of IPA in pristine UiO-66 at 291 K. TraPPE [59] and SKS are united atom forcefields where as OPLS-AA is an all atom force-field.

All the models include non-bonded interactions defined by the Lennard-Jones and Coulombic interactions. The IPA united atom model consists of a hydrogen site, an oxygen site and the two sites of CH_3 groups centered on the carbon atom. A positive net charge equivalent to the -OH group is placed on the carbon atom attached to the hydroxyl group. This makes the IPA molecule electroneutral. The SKS potential uses fixed bond length and bond angles and dihedral potentials for more than three sites. The TraPPE-UA model uses fixed bond length and harmonic bond bending and dihedral potentials. The other force-field studied in the work is optimized potential for liquid simulation All-Atom (OPLS-AA). It is one of the best overall force-field to describe the small organic molecules in liquid phase because of its ability to reproduce the thermodynamic properties such as density, enthalpy of vaporization and many more properties of the liquid phase which is often not easier with AMBER and other force-fields [60]. OPLS-AA is all atom explicit potential with 12 interaction sites for IPA molecule. All atom model allows more flexibility for charge distribution and also for torsional energetics as reported by Jorgensen *et al.*

Further simulations for Defective MOFs have been carried out by using TraPPE-UA IPA potential because it is computationally efficient as there are 5 interaction sites for IPA in United Atom model compared to 12 interaction sites in all-atom model.

3.2 Calculation Methods

We have simulated absolute adsorption isotherm of IPA at 291K in pristine and Defective UiO-66 via Grand Canonical Monte Carlo (GCMC) simulations, using RASPA software. The adsorption isotherms were calculated in 3x3x3 unit cell for pristine, 17% and 33% defective UiO-66. 1x10^5 equilibration cycles followed by 2x10^5 production cycles have been performed for each pressure in the isotherm. Ewald charge method was applied with a cut off of 14 Åand with standard tail corrections. The Ideal Gas Rosenbluth for TraPPE IPA and OPLS-AA IPA model were computed to be 0.2411 and 0.04831 respectively. The relative probabilities for Monte Carlo moves were 1:1:1:2 for translation, rotation, reinsertion and swap probabilities. UFF and DREIDING framework force-fields were used for Pristine UiO-66. The later simulations used only UFF framework potential. The Helium void fraction was calculated to be 0.47508, 0.509683, 0.513973 , 0.533021, 0.58203 for pristine, 4%, 8%, 17% and 33% defect levels in UiO-66.

3.3 Result and Discussion

3.3.1 Impact of Different Fluid and Framework Potentials on the Adsorption of Isopropanol in Pristine UiO-66

We have studied the impact of different fluid potentials and framework potentials on the adsorption of IPA in Pristine UiO-66 at 291 K as shown in Figure 14. The isotherms include three IPA potentials - TraPPE-UA, SKS and OPLS-AA. All the model descriptions have been provided above. The effect of the framework potential has been elucidated by studying the UFF and DREIDING forcefields on TraPPE IPA model. SKS and OPLS-AA use UFF framework potential. From Figure 14, we observe that all the fluid potentials overestimate the NMR results for $\frac{P}{P_0}$ <0.03 whereas underestimate the saturation loading. The reasons for the disagreement in the simulated and experimental results could be due to the presence of defects in the prepared samples of UiO-66 or due to inaccurate framework or fluid potentials.

We have investigated the impact of IPA fluid potentials by studying the adsorption of IPA in Pristine and 17% defect (one missing linker per formula unit). From Figure 15, we can see that OPLS-AA gives lower amount of IPA uptake as compared to TraPPE-UA for both pristine and 17% defect level at high pressure. This can be explained by the reason that TraPPE model is more compact with only 5 interaction sites than OPLS-AA which has 12 interaction sites for IPA molecule.

3.3.2 Adsorption of Isopropanol in Defective UiO-66 for Different Capping Groups

To further explore the reason of disagreement, we studied the adsorption of IPA molecules in defective UiO-66 with different capping groups - hydroxide, formate and acetate as the experimental groups have investigated that the capping groups for their prepared samples were either primarily formate or a mixture of formate and acetate or TFA, based on the modulator they used to prepare the samples. Previously, the experimental groups believed that the capping group was hydroxide and so the GCMC simulations for the OH capped group (two OH groups added for each missing linker to make the Zr open metal cluster fully coordinated) showed an increase in IPA uptake at low pressure with the increase in the defect levels as shown in Figure 16. The adsorption loading increased with the increase in the defect level upto 17% defect (one missing linker per formula unit) at 1 Pa and then decreased for 33% defect (two missing linker per formula unit). At saturation pressure, the amount of IPA uptake increased with the increase in the level of defects for OH capped groups. The IPA uptake is higher in low pressure regime due to increased hydrogen bonding of IPA molecules with the added OH groups and μ_3-OH groups present in the SBUs. To confirm our hypothesis, we tried to find the fraction of molecules hydrogen bonded to μ_3-OH and added OH groups based on our findings that the hydrogen bonding happens at a distance less than 2 Å . According to the Figure 17, more than 50% of total IPA molecules are hydrogen bonded to μ_3-OH and added OH at low pressure. The fraction of IPA hydrogen bonded increases with the increase in the level of defects and decreases with the increase in pressure for the corresponding defect level. However, we are not confident with the hydrogen bonding

analysis as the framework is rigid and for accurate results, the flexibility of the MOF should be considered. Even the hydrogen bonding results with the rigid MOF give us confidence with our adsorption isotherm showing higher IPA uptakes at low pressures.

Since our experimental group confirmed that formate was the major capping group, we modeled 4%, 8%, 17% and 33% defect levels in UiO-66 with formate capping groups (two formate groups for each missing linker). As shown in Figure 18, the molecule adsorption decreases with the increase in the level of defects capped with formate groups in contrast to increase in adsorption loading with the increase in defect levels with OH capped groups (Figure 16) at low pressure. At high pressure, saturation loading increases with the increase in the level of defects for both OH and formate capped groups. We have also simulated adsorption of IPA in 17% defective UiO-66 capped with acetate group (two acetate groups for each missing linker). From the comparison plot (Figure 19), the adsorption in acetate capped 17% defective UiO-66 resembles that of Pristine at low pressure. The higher pressure loading for acetate group is in between formate and Pristine adsorption loading. This is because in low pressure regime, the physics of the isotherm is dominated by the available surface area. Thus, the adsorption is highest for Pristine followed by acetate and then formate capped Defective UiO-66. The OH group has highest adsorption loading due to the formation of the hydrogen bonding of IPA molecules with the OH capped group and μ_3-OH at low pressure. At high pressure regime of the isotherm, the adsorption is controlled by free volume which is higher for OH capped followed by formate capped and then acetate and lastly Pristine UiO-66.

Lastly we have found an approximate range of the defect in the synthesized UiO-66 sample by the experimental group. From Figure 20, we observe that 8% formate capped defective UiO-66 is in good agreement with the experiments in the low pressure regime. However, it under predicts the experimental saturation loading for $\frac{P}{P_0} > 0.2$ and 17% defect level simulation over predicts the loading at high pressure. Thus, the experimental results can be achieved by defect level in between 8% and 17% defect level.

3.4 Conclusion

We studied the adsorption of isopropanol at 291 K in Pristine UiO-66 using different IPA models and framework potentials. All types of adsorbate potentials showed higher uptake than the NMR results for $\frac{P}{P_0}$ <0.03 and lower uptake for pressure beyond that. This reveals that either the potentials are unable to capture the adsorption accurately or the synthesized UiO-66 possesses some level of defects which exists in real life. We modeled adsorption of IPA in Defective UiO-66 and studied the impact of different capping groups and level of defects. We have also studied the impact of missing linker defect level on the hydrogen bonding of IPA with the metal cluster. The standard UFF framework potential does not account for hydrogen bonding. We have created modified potential to allow hydrogen bonding between IPA and UiO-66 framework atoms. The adsorption of IPA increased with the increase in defect levels due to hydrogen bonding of IPA with μ_3-OH groups for hydroxide capped group. We have shown that the fraction of IPA hydrogen bonded to μ_3-OH is a function of pressure in all level of defects. The hydrogen bonding increases with the increase in the level of defects due to more number of added OH groups. We then studied the adsorption of IPA in formate capped groups with different level of defects in UiO-66. Finally, we studied the impact of different capping groups on the adsorption of IPA in 17% defect. The adsorption was highest for hydroxide capped group due to hydrogen bonding, followed by pristine, then acetate and finally formate capped group at low pressure due to available surface area argument. The high pressure regime of the isotherm was governed by the free volume and so the order exactly flipped. According to the comparison plot of experimental adsorption isotherm with the modeling, we believe that the synthesized UiO-66 framework has a defect level in between 8-17%.

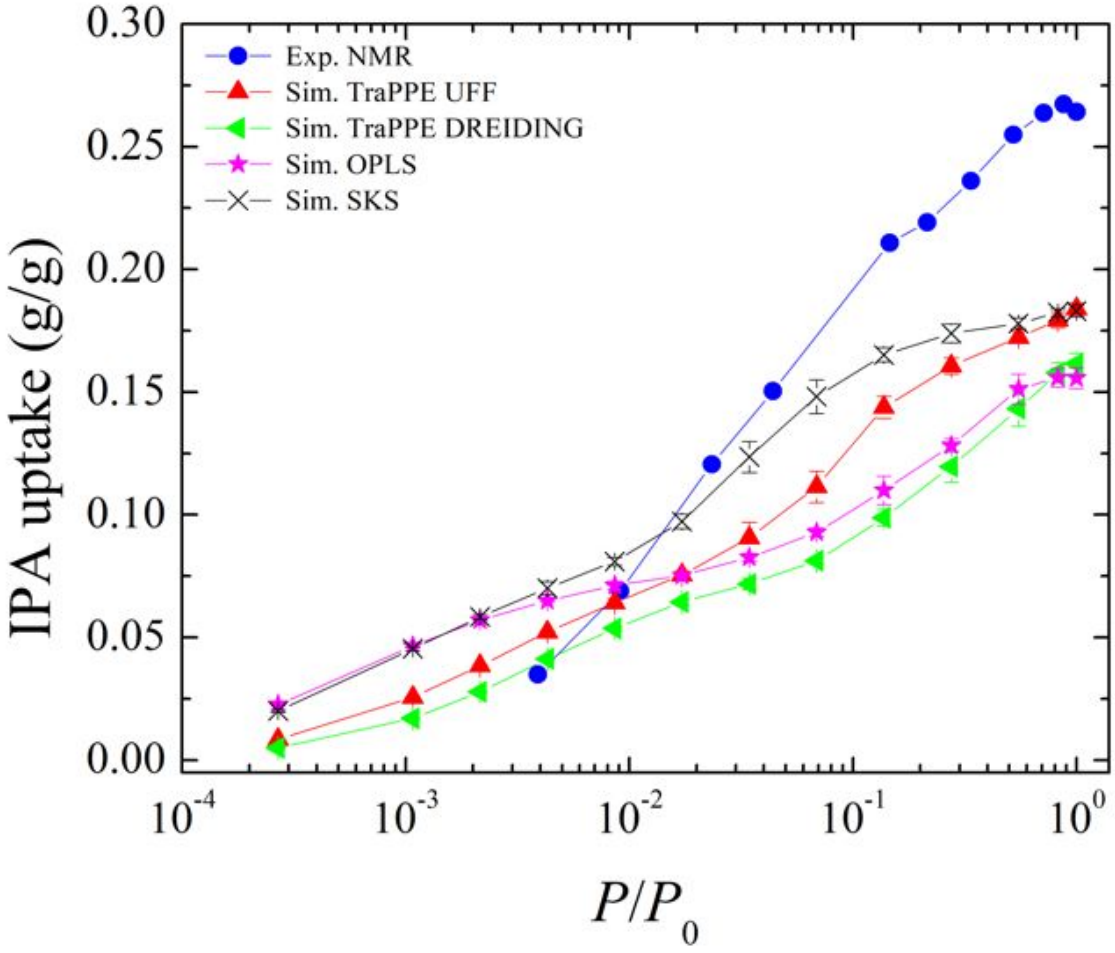

Figure 14: Adsorption isotherm of isopropanol at 291 K via GCMC simulations for various molecule (TraPPE, SKS and OPLS-AA) and framework (UFF and DREIDING) potentials and NMR experiments

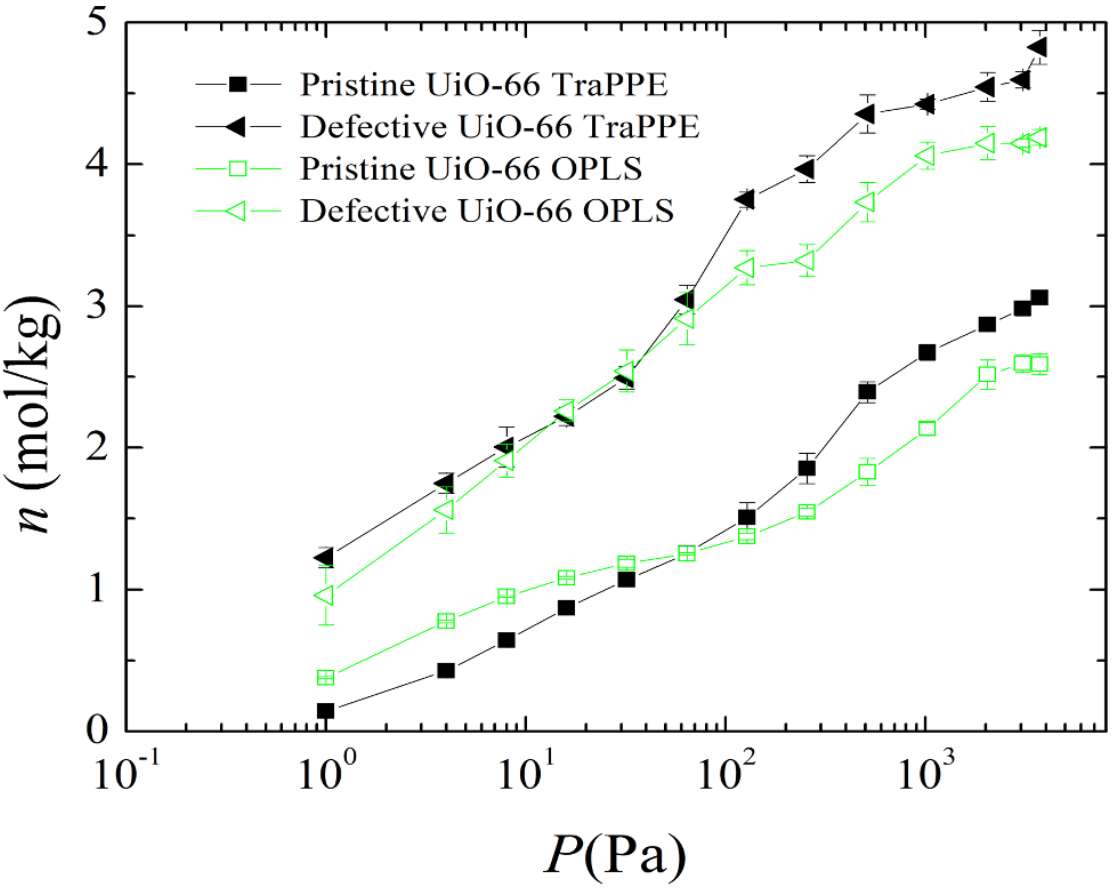

Figure 15: Adsorption isotherm for IPA at 291 K via GCMC simulations at 17% defect with OH capped group and two IPA potentials - TraPPE and OPLS-AA

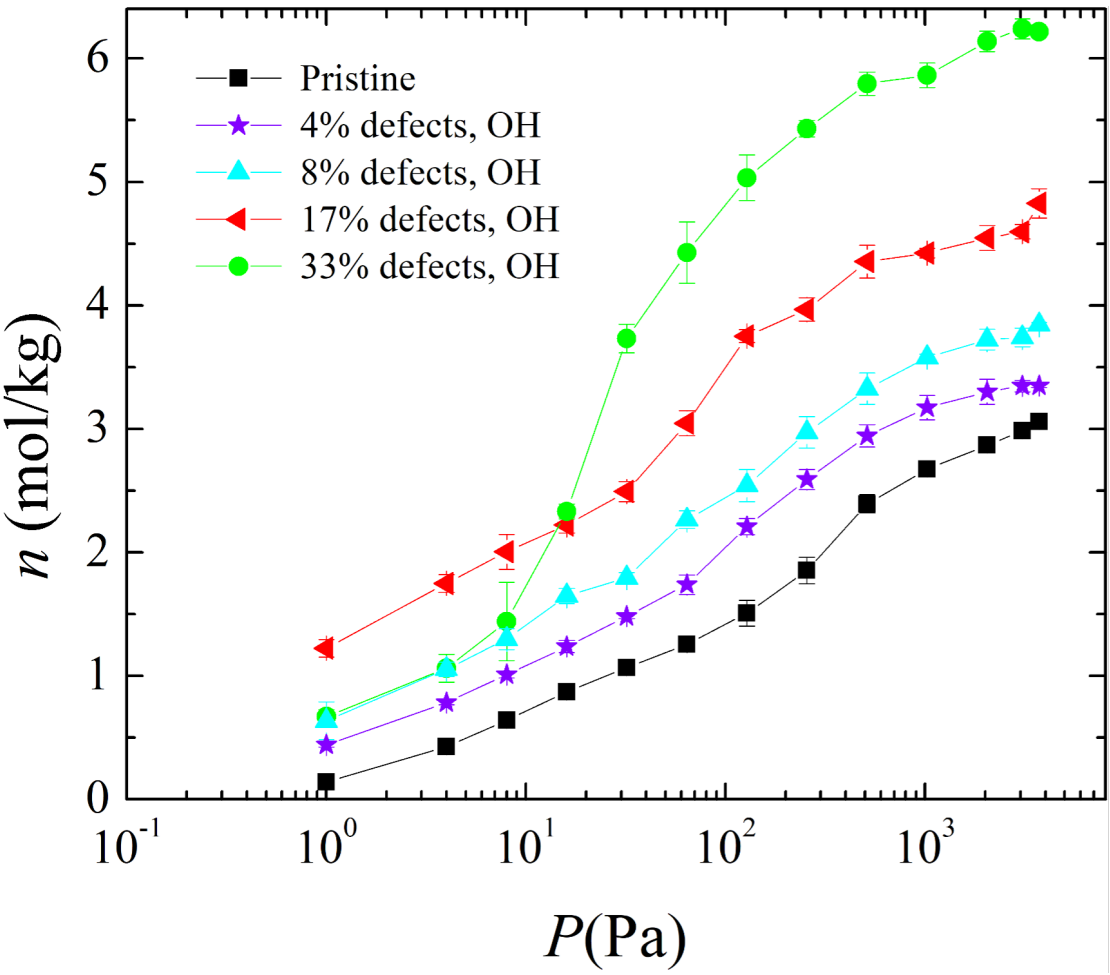

Figure 16: Adsorption isotherm for IPA at 291 K via GCMC simulations with several level of missing linker defects in UiO-66 and added OH capping group

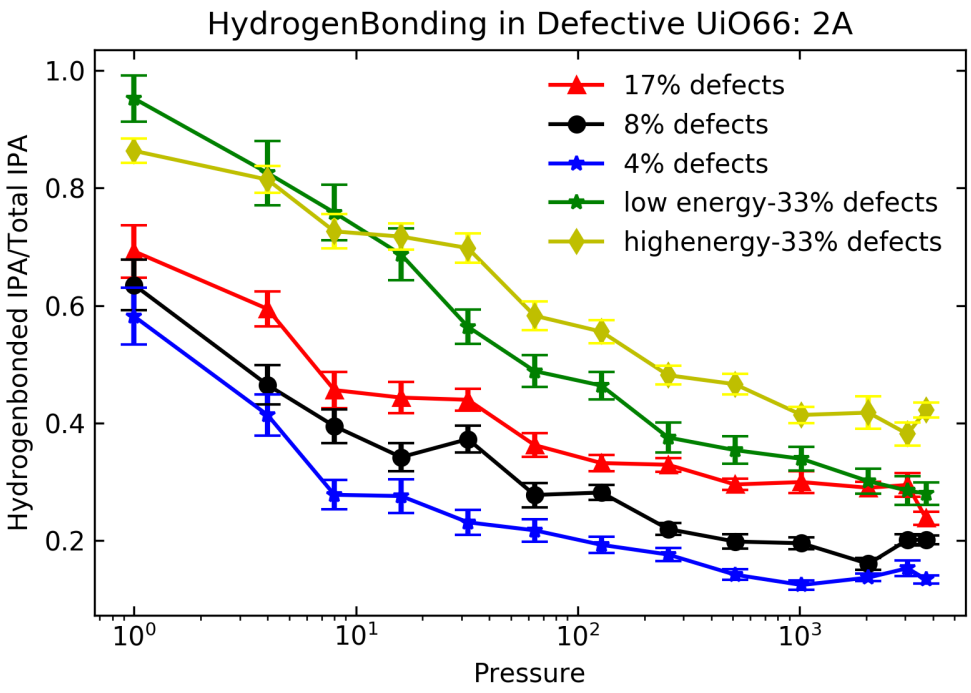

Figure 17: Fraction of IPA molecules hydrogen bonded to μ_3-OH and added OH groups in several level of missing linker defects in UiO-66

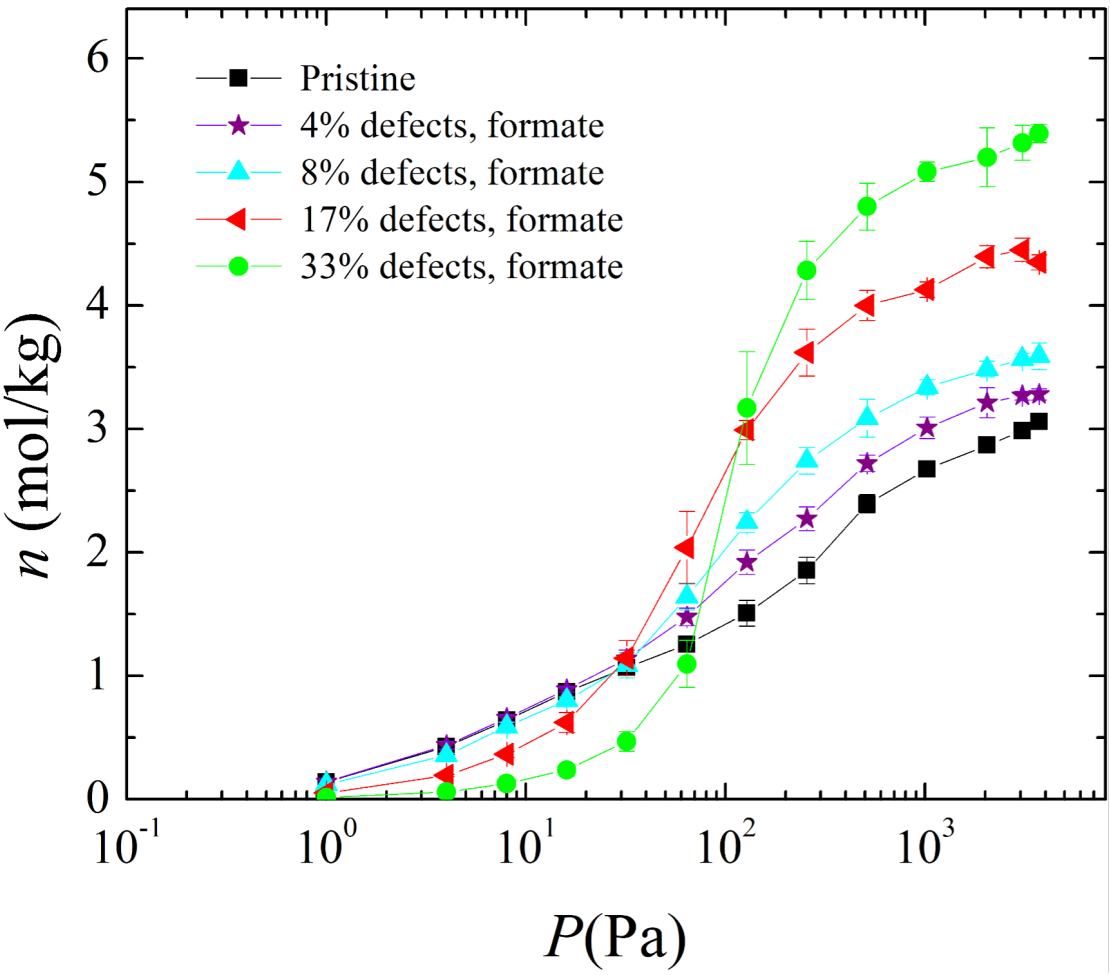

Figure 18: Adsorption isotherm of IPA at 291 K via GCMC simulations with several level of missing linker defects in UiO-66 and formate capping group

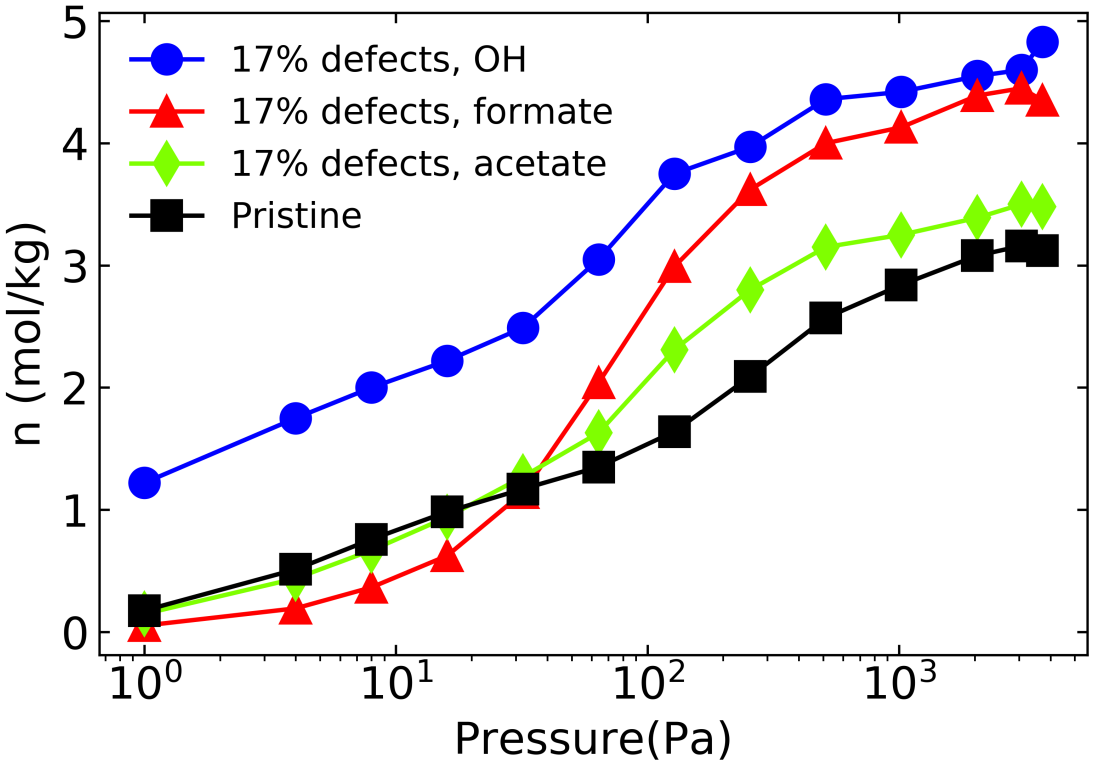

Figure 19: Adsorption isotherm of IPA at 291 K via GCMC simulations for Pristine, 17% defective UiO-66 capped with addedOH, formate and acetate groups

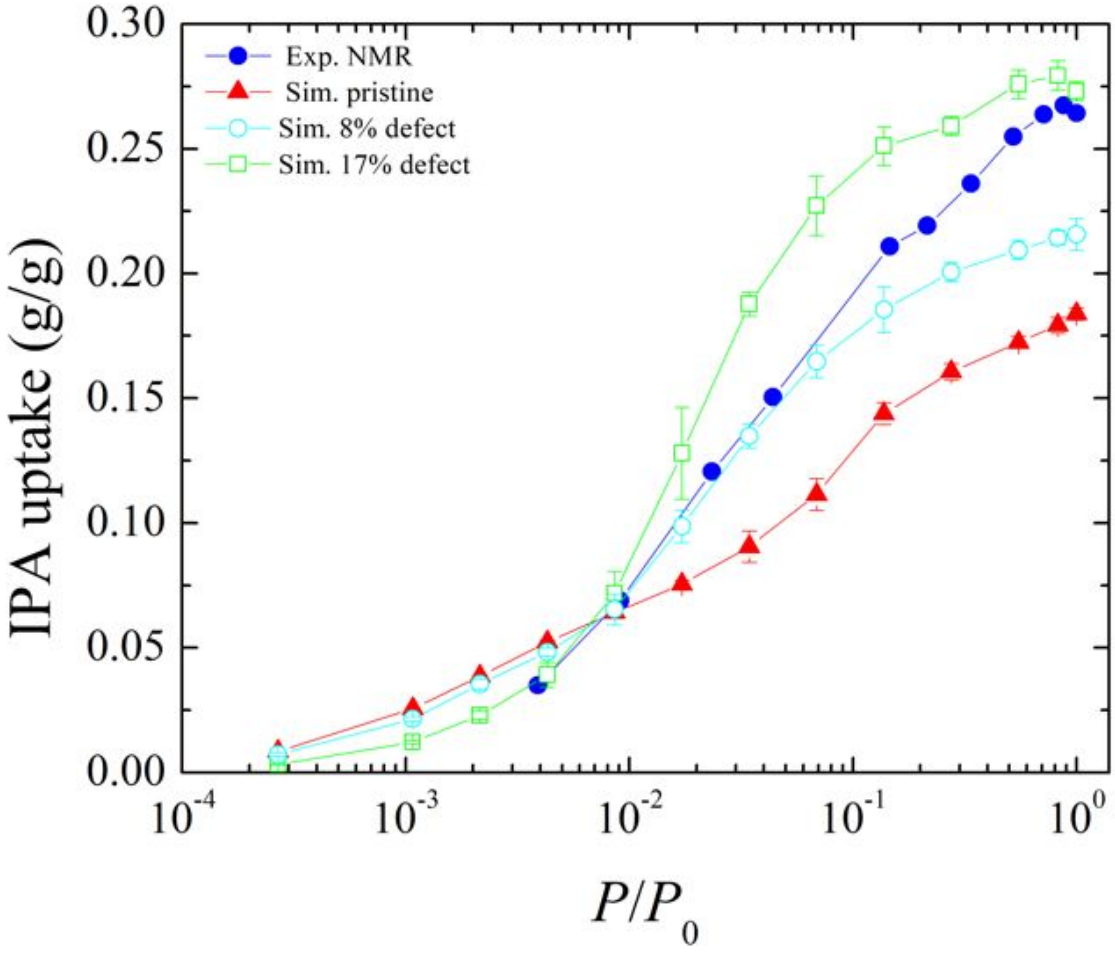

Figure 20: Adsorption isotherm for IPA at 291 K via GCMC simulations for Pristine, 8% and 17% formate capped defective UiO-66 and NMR experimental results

4.0 Adsorption of Acetone in Pristine and Defective-UiO66

4.1 Introduction

In this work, we have studied the adsorption of acetone in pristine UiO-66 before exploring the effect of missing linker defects on adsorption. We chose acetone as our guest molecule because of its small size and ability to form hydrogen bonds only with the SBUs.

Wardzala et al. [61] reported the diffusion of Acetone in UiO-66 and that the standard UFF Lennard Jones terms does not include the hydrogen bonding of the μ_3-OH with the guest molecules. This is because the Lennard Jones parameter for hydrogen in the μ_3-OH restricts the oxygen atom of acetone from coming closer than about 2.8 Å; whereas hydrogen bonds are formed at distance less than 2 Å. The findings have been confirmed by the DFT calculations where they've reported the hydrogen bonding distance of 1.8 Åbetween H atom of μ_3-OH group and oxygen atom of the acetone molecule. Thus, adsorption isotherms for this work have been studied by modifying the standard UFF Lennard Jones parameters for H and O atom of μ_3-OH and replacing with O and H parameters of the TraPPE isopropanol potentials.

4.2 Calculation Methods

The acetone in Pristine and Defective UiO-66 is simulated with 70000 equilibration cycles and $1x10^5$ production cycles. The Ideal Gas Rosenbluth weight of acetone was calculated to be 1.01. We have used the TraPPE-UA model of acetone to model the adsorption [62]. A cut-off of 14 Å was applied with standard tail corrections. The interactions were defined by the Lennard-Jones parameters along with Lorentz-Berthlot mixing rule for unlike pairs. Ewald summation method was used. Standard UFF framework potential was used with slight modification to incorporate hydrogen bonding phenomenon of acetone molecules with the framework atoms. 1:1:1:2 relative translational, rotational, reinsertion and swap probabilities

were used. The charges for the UiO-66 framework atoms were computed using DDEC6. The super cell of 3x3x3 cell was used to model adsorption in Pristine UiO-66. The adsorption of acetone was also studied in Defective UiO-66 with 4%, 8%, 17% and 33% defect levels and different capping groups such as hydroxide, formate and acetate groups. The super-cell of 2x3x3 was used for 4% and 8% defective UiO-66 while the rest was done with 3x3x3 super-cell.

4.3 Result and Discussion

4.3.1 Adsorption of Acetone in Pristine UiO-66 at 298 K

We have simulated adsorption isotherm of acetone in Pristine UiO-66 at 298K and up to 10^5 Pa pressure as shown in Figure 21. The saturation vapor pressure of acetone is 30.6 kPa. The acetone is modeled using TraPPE-UA force-field as described in the calculation method section. From Figure 21, there are 5.93 $\pm$ 0.13 molecules of acetone per unit cell at saturation pressure. To expore very high of acetone beyond saturation pressure, we have done simulations at 100, 1000,10000 and 100000 kPa which gave absolute loading of 5.90 $\pm$ 0.1, 5.94 $\pm$ 0.2, 6.1 $\pm$ 0.4, 7.4 $\pm$ 0.1 respectively. The high pressure simulation uses configuration biased Monte Carlo moves. The framework should be modeled flexible at very high pressure. The impact of framework flexibilty on adsorption has been studied in the later section. In our published paper, we have shown that the acetone molecules hydrogen bond with μ_3-OH groups of framework.

4.3.2 Adsorption of Acetone in Defective UiO-66 for Different Capping Groups

We have modeled adsorption of acetone in missing linker defects in UiO-66 capped with OH groups (two hydroxide groups for eaching missing linker). As shown in Figure 22, we have simulated 4%, 8% and 17% defect levels capped with OH groups and compared their adsorption loading with that in Pristine UiO-66. The saturation loading at 100 kPa for Pristine, 4%, 8% and 17 % is 82.8 $\pm$ 1.47, 90.0 $\pm$ 1.0, 97.9 $\pm$ 3.01 and 116.0 $\pm$ 2.39

respectively. The absolute loading increases with the increase in defect level due to the hydrogen bonding between acetone molecules and μ_3-OH and added OH groups. At low pressure i.e. P $<$ 100 Pa, the loading is higher for Pristine followed by increasing level of defects. The loading order reverses after a cross-over as it depends on the free volume at high pressure which is higher for 17% defect level. Our experimental groups have studied adsorption of acetone in UiO-66 which used primarily formic acid or TFA as modulator. Thus, we have studied adsorption in UiO-66 capped with formate groups (two formate for each missing linker to saturate open Zr metal sites) as shown in Figure 23. The behaviour of isotherm is similar to that of OH capped Defective UiO-66 with a intersection at about 100 Pa as seen for adsorption in OH capping results. However, the saturation loading is slightly lower for formate capping than OH capping group because now the hydrogen bonding is only between acetone and the μ_3-OH groups of UiO-66 framework. The loading at 100 kPa for Pristine, 4%, 8% and 17% is 82.8 $\pm$ 1.47, 88.0 $\pm$ 0.95, 97.0 $\pm$ 0.98, and 111.0 $\pm$ 1.94 respectively. We have also tried to find the level of defect which gives the absolute saturation loading close to our experimental data. Our colleagues believe that they have synthesized Pristine UiO-66 but for real materials there is some level of defect present in the material. Figure 24, shows experimental adsorption and desorption isotherms with closed and open squares respectively. Our modeled adsorption in Pristine UiO-66 underpredicts the experimental adsorption isotherm indicating some level of defect. As we can see, the adsorption isotherm is in good agreement with 8% defect capped with the formate groups. Thus, we believe that the synthesized UiO-66 might have possessed 8% defect.

4.4 Conclusion

We have studied the adsorption of acetone in Pristine and Defective UiO-66 capped with different modulators at 298K. The adsorption of acetone beyond high saturation pressure is modeled accurately with introducing the flexibility in the framework atoms. The adsorption of acetone in hydroxide and formate groups increases with the increase in the level of defect at high pressure. However, the amount of acetone adsorbed differs slightly for OH and

formate capping groups. This is due to the triangular planar geometry of acetone and thus the chemistry is different than that of isopropanol. We have compared our results with the experimental results and deduced that the synthesized UiO-66 material might have about 8% defect level.

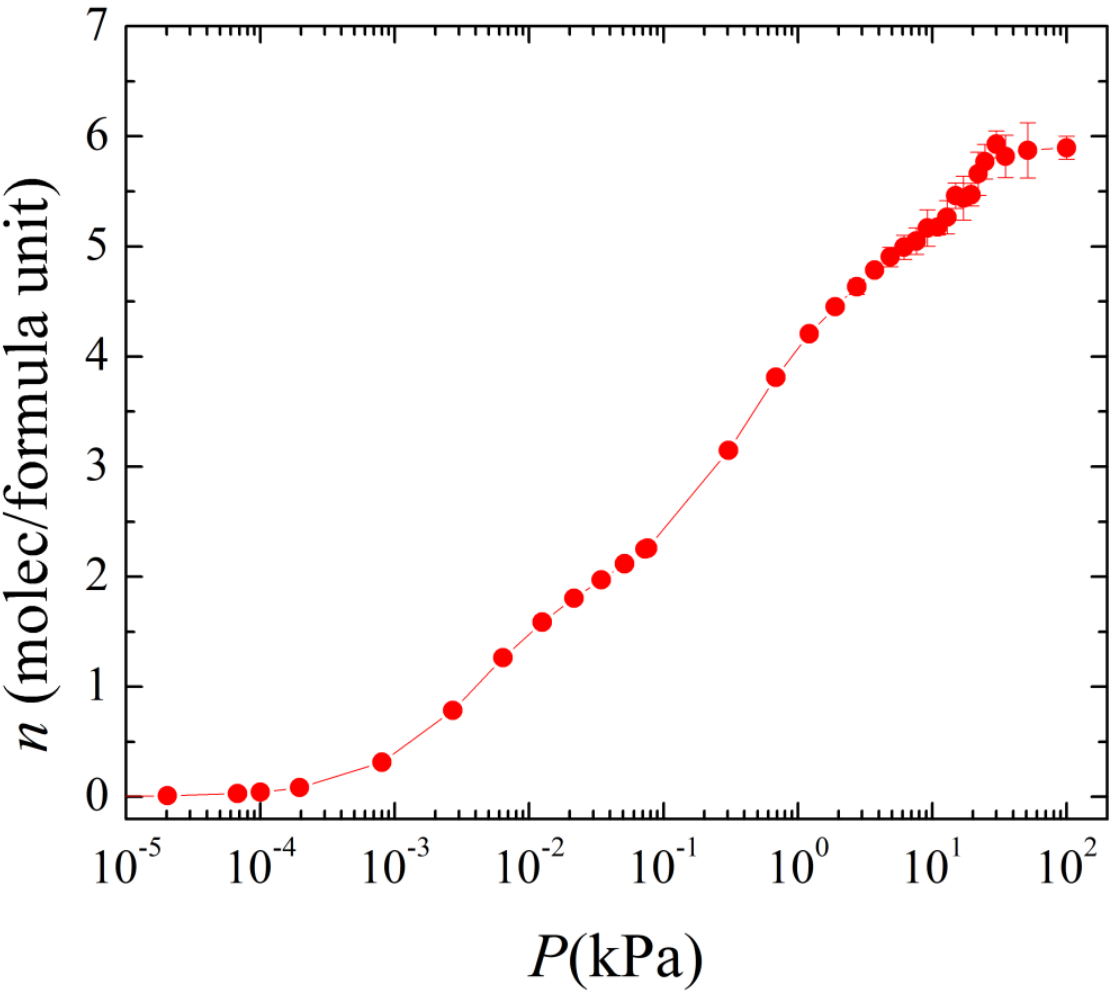

Figure 21: Adsorption isotherm for acetone at 298 K via GCMC simulations in pristine UiO-66

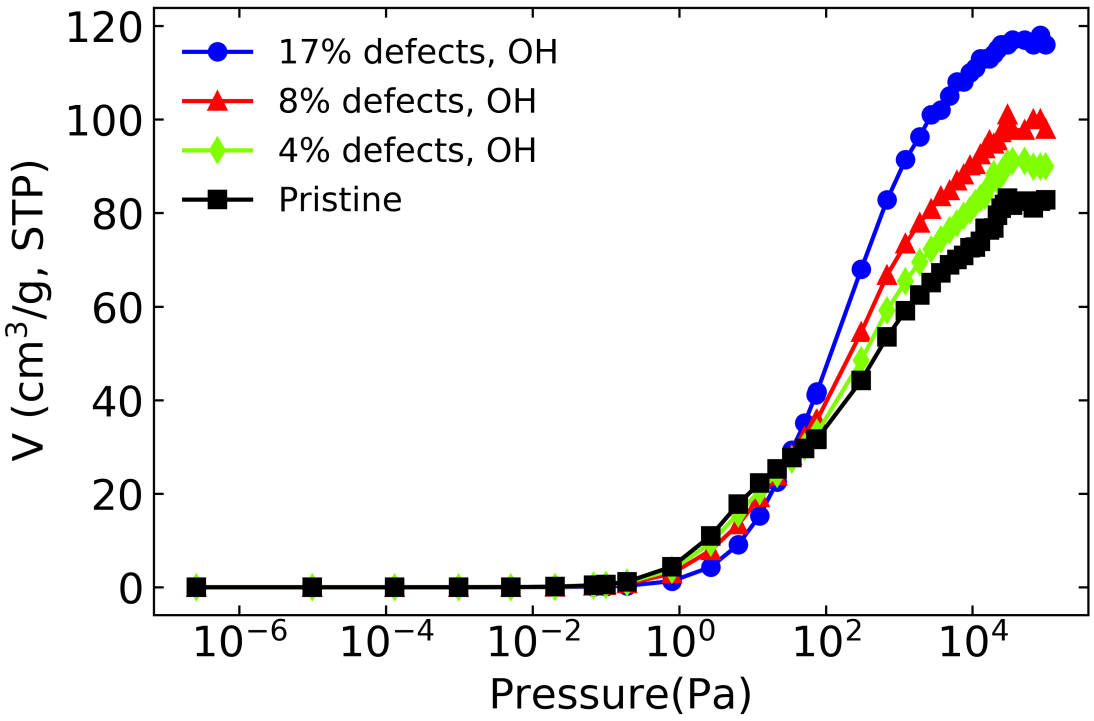

Figure 22: Adsorption isotherm for acetone at 298 K via GCMC simulations in pristine and all defect levels capped with OH group

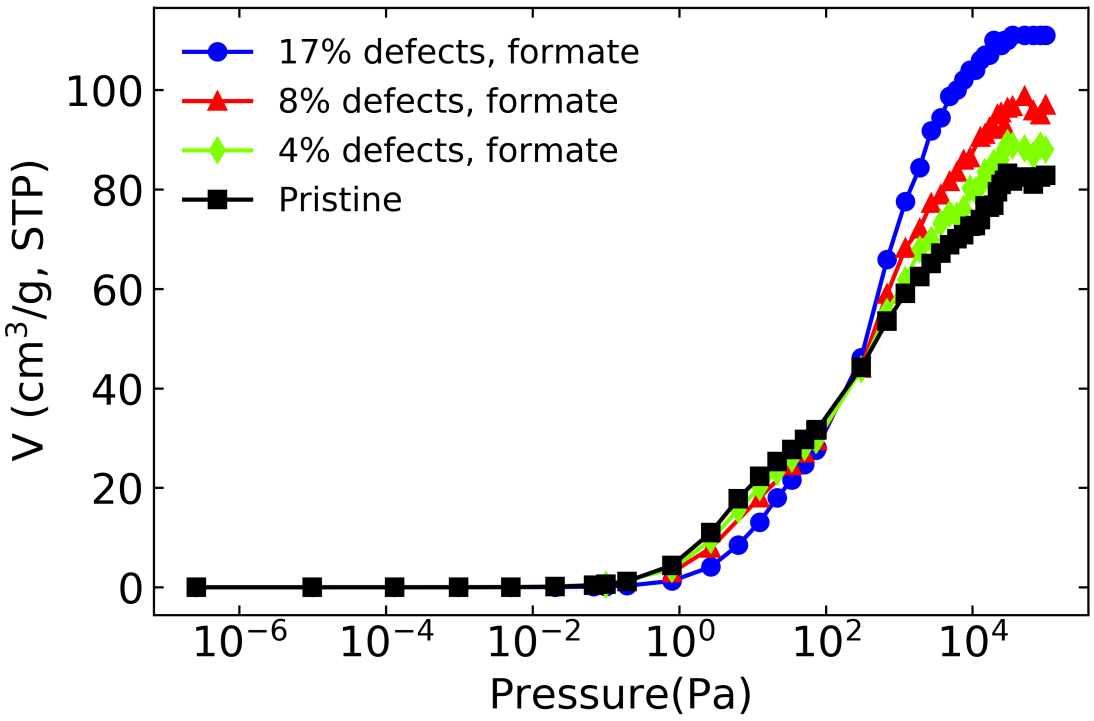

Figure 23: Adsorption isotherm for acetone at 298 K via GCMC simulations in pristine and defect levels capped with formate group

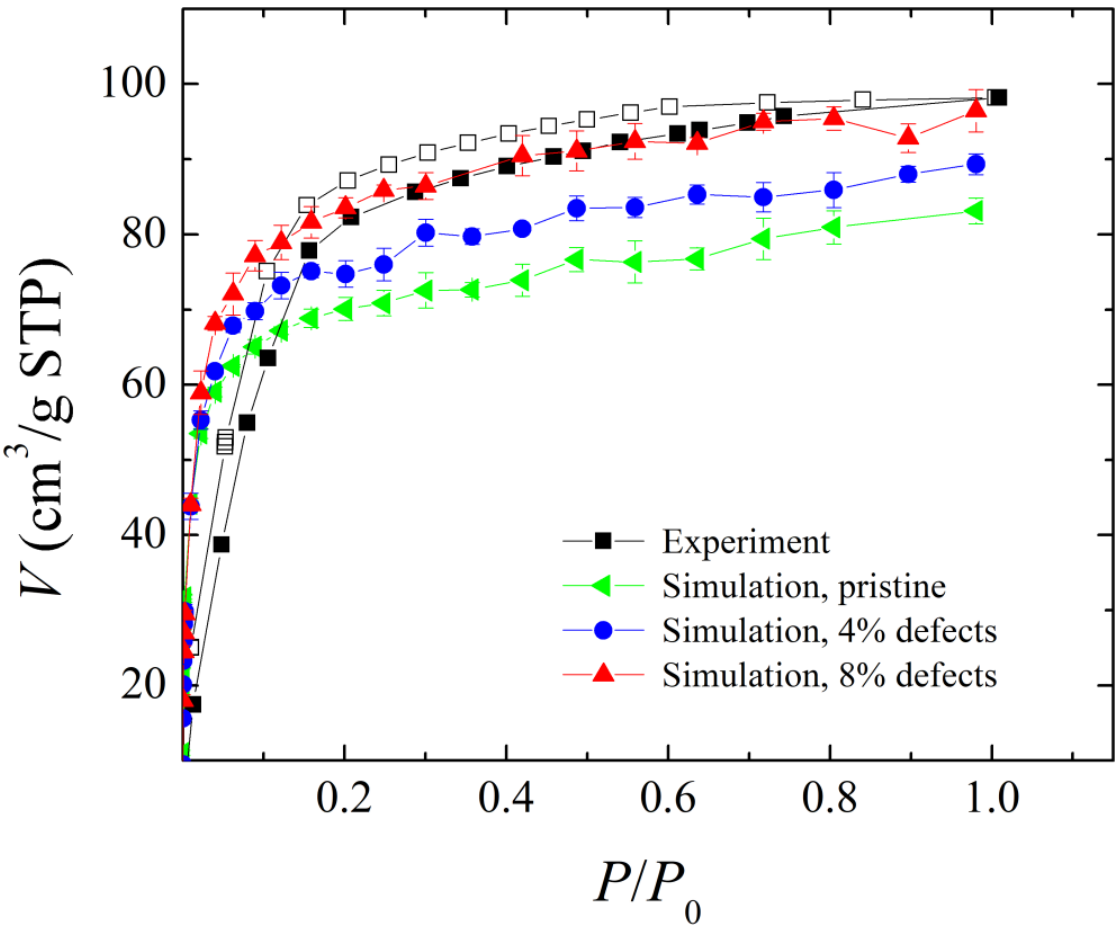

Figure 24: Adsorption isotherm for acetone at 298 K via GCMC simulations for pristine, experiments and 4% and 8% formate capped defective UiO-66

5.0 Impact of Intrinsic Framework Flexibility on the Adsorption of Molecules in UiO-66

5.1 Introduction

Molecular modeling is used to study the adsorption of molecules in various MOFs [63, 64, 65, 66, 67]. However, the modeling of adsorption of molecules in MOFs is often done by holding the MOF structure rigid. This increases the computational efficiencies [68, 69, 70, 71]. During the adsorption of molecules, some MOFs undergo structure deformation such as swelling or transition between bi-stable states[72] whereas some of them do not show any change in the volume. Despite this, all MOFs undergo slight displacement due to the thermal vibrations of the framework atoms [73, 74, 75]. This phenomenon is known as the intrinsic flexibility of the framework atoms as reported by Jongwoo et al [76]. This intrinsic framework flexibility has a significant impact on the adsorption modeling as reported by several studies [77, 78, 79, 80]. All the published works have shown the impact of intrinsic framework flexibility by creating an ensemble of empty frameworks. However, our hypothesis is that the structure of any MOF linker would be perturbed by the presence of guest molecules in the ensemble. This would lead to a significant difference in the configuration of the empty and finite loaded MOFs with the guest molecules. To test our hypothesis, we have studied the impact of intrinsic framework flexibility on the adsorption of acetone and nitrogen guest molecules in Pristine UiO-66 by performing GCMC simulations on NVT MD generated snapshots of empty UiO-66 framework and 7 loading acetone in UiO-66.

5.2 Calculation Methods

5.2.1 NVT-MD

The snapshots for modeling adsorption was done by performing NVT MD simulations of empty UiO-66 framework and 7 loading acetone per unit cell in UiO-66 using classical forcefields [81] in LAMMPS software. The method of generating snapshots was studied by Gee et al [79, 80] but it was performed only for empty framework structures and not for the snapshots created by generating an ensemble of molecules present in the UiO-66 framework. NVT MD simulations were performed using LAMMPS software [82] at 298K and with a timestep of 1.0 fs. The MD simulations were done for empty and finite loading of acetone in the framework. The simulations used 2x2x2 supercell of UiO-66 that consists of 32 primitive cells with each formula unit consisting of one octahedral and two tetrahedral pores. We have used flexible TraPPE/Rogge classical potential [83] to describe the UiO-66 forcefield. The charges were computed by DDEC6 and Chargemol programs for Rogge potential. Periodic boundary conditions were applied in all the directions with a cutoff of 12.5 Å. Hybrid mm3 Harmonic bonding and harmonic angle potentials were used for the framework atoms modeled with 7 loading of acetone. For bonds separated by more than 3, hybrid OPLS fourier torsion potentials were used. The acetone was modeled by using TraPPE-UA potential. The system was equilibrated by a Nose-Hoover thermostat [84, 85] for 100 ps in NVT ensemble with a decay period of 0.1 ps. The paper by Agrawal et al. [80] uses production run of 1 ns with the snapshots taken every 100 ps. For better uncorrelated MD snapshots [80], the data consisting of only framework atoms coordinates and charges were dumped from the production run of 2 ns in the NVT emsemble for every 100 ps. This gave us 20 snapshots representing intrinsically flexibility in empty and 7 loaded acetone UiO-66 framework. Some studies have also shown an alternative procedure of generating snapshots via ab initio MD simulations [86, 87]. However, DFT MD simulations are more computationally expensive than classical MD potentials.

5.2.2 GCMC Simulation for Modeling the Adsorption of Molecules in Intrinsic Flexible UiO-66

We have performed the adsorption of acetone at 298 K and N_2 at 77 K molecules via GCMC simulations using RASPA software. TraPPE potentials were used for both the molecules. The adsorption isotherms for acetone and N_2 were also performed on DFT minimized rigid UiO-66. 11 MD generated snapshots were used to model the adsorption isotherm simulations in empty and 7 loading of acetone UiO-66 framework. Each snapshot was held rigid during the simulations. A cubic unit cell of box length 41.9568 Å was used consisting of 3648 UiO-66 framework atoms. This unit cell had 32 formula units with four primitive cells in each formula unit. $1x10^5$ equilibration cycles along with 70,000 production cycles were used to simulate each pressure in the acetone adsorption isotherm where each cycle consisted of N steps and N is the number of adsorbate molecules. For simulating N_2 adsorption isotherm, 8000 equilibration and production cycles were used for each pressure. 8000 equilibration cycles were enough to equilibrate the system as shown in the Results and discussion below. The cutoff radius of 14 Å along with standard tail corrections was used for both acetone and N_2 systems. UFF and TraPPE Lennard-Jones parameters were used to compute the van der Waals interactions and electrostatic interactions of adsorbate-adsorbate and adsorbate-adsorbent molecules. WE have used modified UFF potential to include the hydrogen bonding of the adsorbate-adsorbents atoms. The unlike pair interactions were defind by Lorentz-Berthelot mixing rules. Ewald summation method was used to calculate the electrostatic potentials. Swap, transational, reinsertion and rotation moves were applied in the ratio of 2:1:1:1. The Helium void fraction for the DFT minimized structure was calculated to be 0.508064. The Helium void fractions for all snapshots were also calculated and are discussed below. The ideal gas Rosenbluth weight for acetone and N_2 are 1.01 and 1.0 respectively. The GCMC simulations of each snapshots generated from MD simulated were averaged to model adsorption of molecules in intrinsic flexible MOFs. We have used 11 snapshots to model the adsorption and these number of snapshots are enough to produce converged results as reported by Agrawal et al [80].

5.3 Result and discussion

We have compared the adsorption isotherms of N_2 at 77 K for RASPA triclinic cell and DFT minimized crystallographic structure of rigid UiO-66 framework. The RASPA unit cell lattice parameter are: a = b = c = 14.834 Å , $\alpha = \beta = \gamma = 60°$, cell volume = 62319.45 $Å^3$, box-length = x = y = z = 44.5020 Å for 3x3x3 super-cell used in the simulations. DFT minimized crystallographic structure is a 2x2x2 cubic super-cell with 32 primitive cells and cell parameters, a = b = c = 41.9568 Å (each primitive cell a=b=c=13.9856 Å) , $\alpha = \beta = \gamma = 90°$, cell volume = 73859.62 $Å^3$. To compare DFT structure consisting 32 primitive cell volume with RASPA triclinic cell, 4x4x2 super-cell has a volume of 73860.086 $Å^3$ and box-length = x = y = 59.336, z = 29.6680.

5.3.1 Impact of Intrinsic Framework Flexibility on the Adsorption of Nitrogen in Empty and Finite Adsorbent Loaded UiO-66 Framework

The N_2 adsorption isotherms in RASPA triclinic cell and DFT minimum energy structure are in good agreement in low pressure and high pressure regime as shown in Figure 27. The uptake in the intermediate region is slightly higher for DFT structure than RASPA triclinic cell due to higher volume. The saturation loading of N_2 is 296.32 cm^3/g for both the cells. From Figure 25, we can observe that 8000 equilibration cycles are sufficient to equilibrate the system for all the snapshots used for running GCMC simulation of N_2 in intrinsic flexible UiO-66 framework. We have also calculated the Helium void fraction of the 7 loaded acetone MD generated snapshots used in the calculations and found that there is no correlation between the N_2 saturation loading and the Helium void fraction as shown in Figure 26.

5.3.2 Impact of Intrinsic Framework Flexibility on the Adsorption of Acetone in Empty and Finite Adsorbent Loaded UiO-66 Framework

The adsorption isotherm of acetone at 298 K in DFT minimized structure and RASPA triclinic cell are also in good agreement within the error bars in low pressure and high pressure regime. The adsorption of acetone for pressure above the saturation in DFT structure is

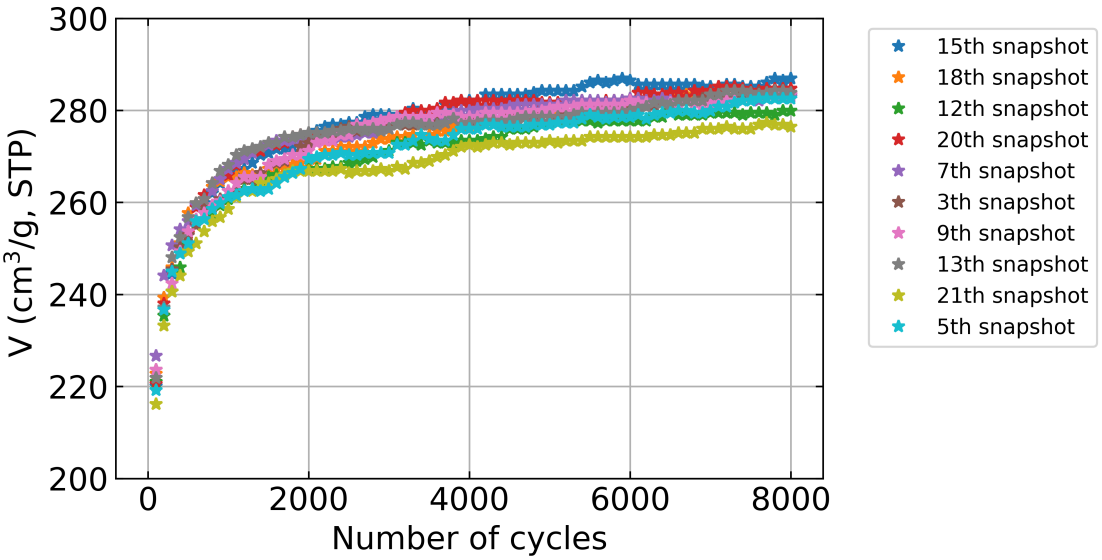

Figure 25: Equilibration plot of nitrogen in 7 loading of acetone in UiO-66 MOF snapshots at 101430 Pa

3.70 ± 0.059, 3.64 ± 0.11 and 3.82 ± 0.19 at 1, 10 and 100 bar. The adsorption of acetone for pressure above the saturation for RASPA triclinic cell is 3.69 ± 0.065, 3.72 ± 0.12 and 3.82 ± 0.23 at 1, 10 and 100 bar. We have also studied the adsorption of acetone in empty UiO-66 and 7 loading of acetone in UiO-66 frameworks MD snapshots. The average of all the snapshots represent intrinsic flexible framework. Figure 29 shows the comparison plot of adsorption of acetone in DFT minimized structure, empty framework and 7 loading of acetone in framework. The acetone uptake is lower for rigid DFT minimized structure as there is no movement of organic linkers in the presence of an adsorbate. Flexible framework shows higher adsorption loading than rigid DFT minimized structure due to different orientations of the organic linker. The loading of acetone is highest for acetone loaded MD structures. However, the saturation N_2 uptake is lower in 7 loaded acetone frameworks as seen before. Thus, acetone loaded MD structures accommodate more acetone but not more N_2 molecules. This suggests that one should do MD simulations of the molecule in order to measure the isotherm. The saturation loading of acetone in empty framework is 3.94 ± 0.07, 3.94 ±

0.08 and 4.05 ± 0.089 at 1, 10 and 100 bar. The saturation loading of acetone in 7 loading acetone framework is 4.33 ± 0.051, 4.33 ± 0.046 and 4.38 ± 0.073 at 1, 10 and 100 bar. This confirms that the framework flexibility has a significant impact on the adsorption ability with the presence of similar molecules in the framework.

5.4 Conclusion

We have studied the impact of intrinsic framework flexibility on the adsorption of acetone and N_2 by creating an ensemble of empty and acetone loaded frameworks. We have performed GCMC simulations using independent NVT MD snapshots of empty and loaded frameworks by holding each snapshot rigid. We have averaged each independent GCMC simulations of the guest molecules in empty and highly loaded acetone in UiO-66 MD snapshots to model the intrinsic flexibility in the MOF. N_2 saturation loading is always lower in loaded acetone snapshots. The adsorption of acetone increases at high saturation pressure in 7 loaded acetone MD snapshots, followed by empty framework MD snapshots and finally in DFT minimized structure. This implies that one should perform MD simulations of the molecule for which we want to measure the adsorption isotherm.

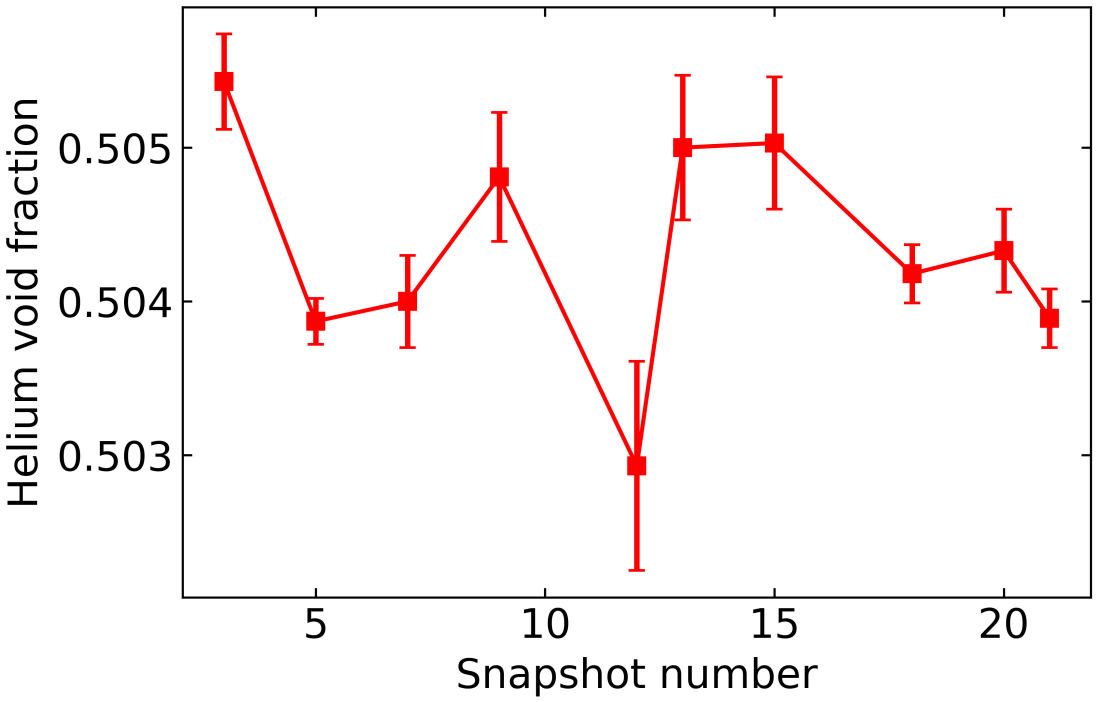

Figure 26: Helium void fraction of 7 loading acetone in UiO-66 MOF snapshots

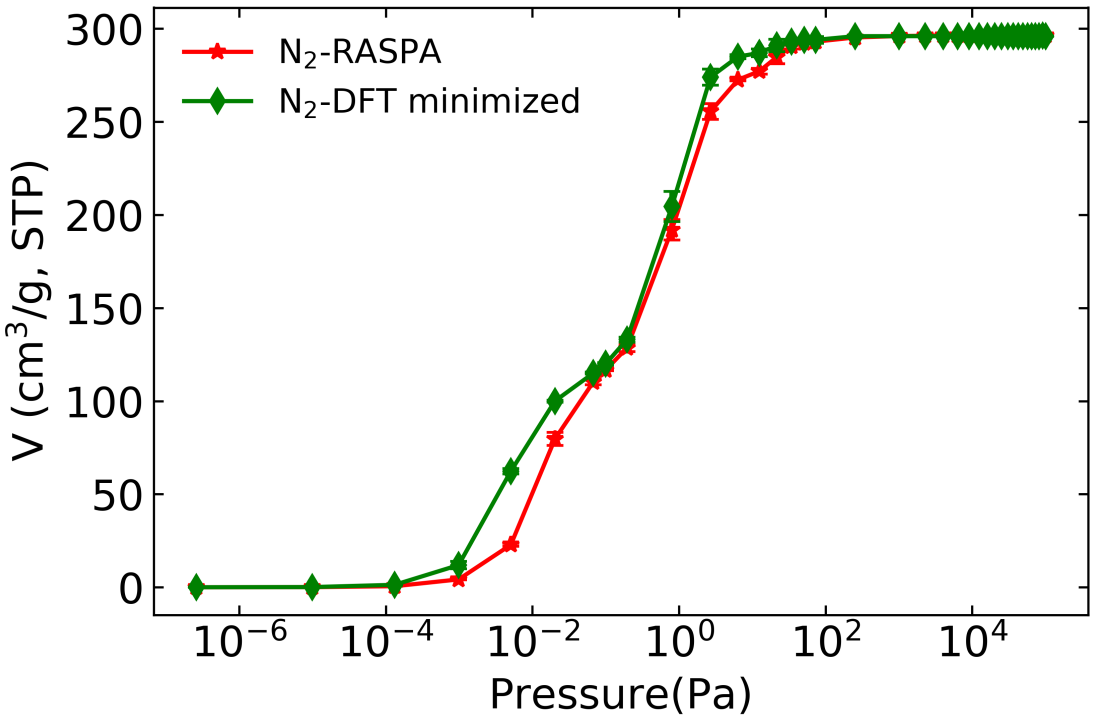

Figure 27: Adsorption isotherm of nitrogen at 77 K in DFT minimized structure, and RASPA triclinic cell

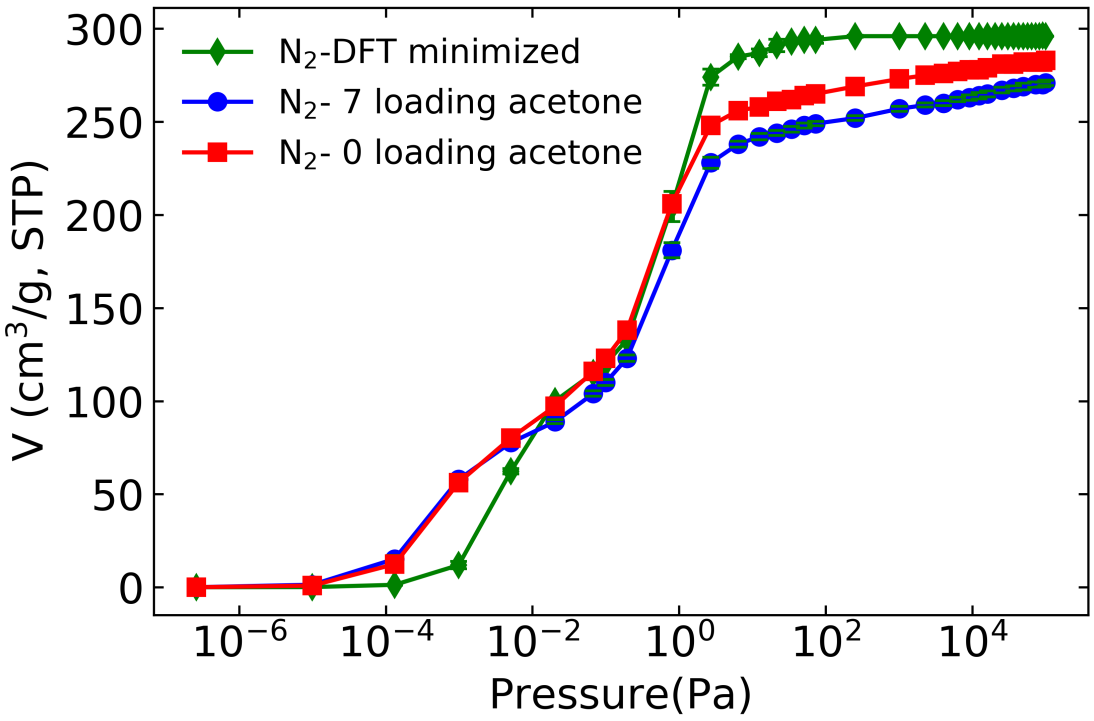

Figure 28: Adsorption isotherm of nitrogen at 77 K in LAMMPS DFT minimized structure, 7 loading of acetone in UiO-66 and empty UiO-66 framework

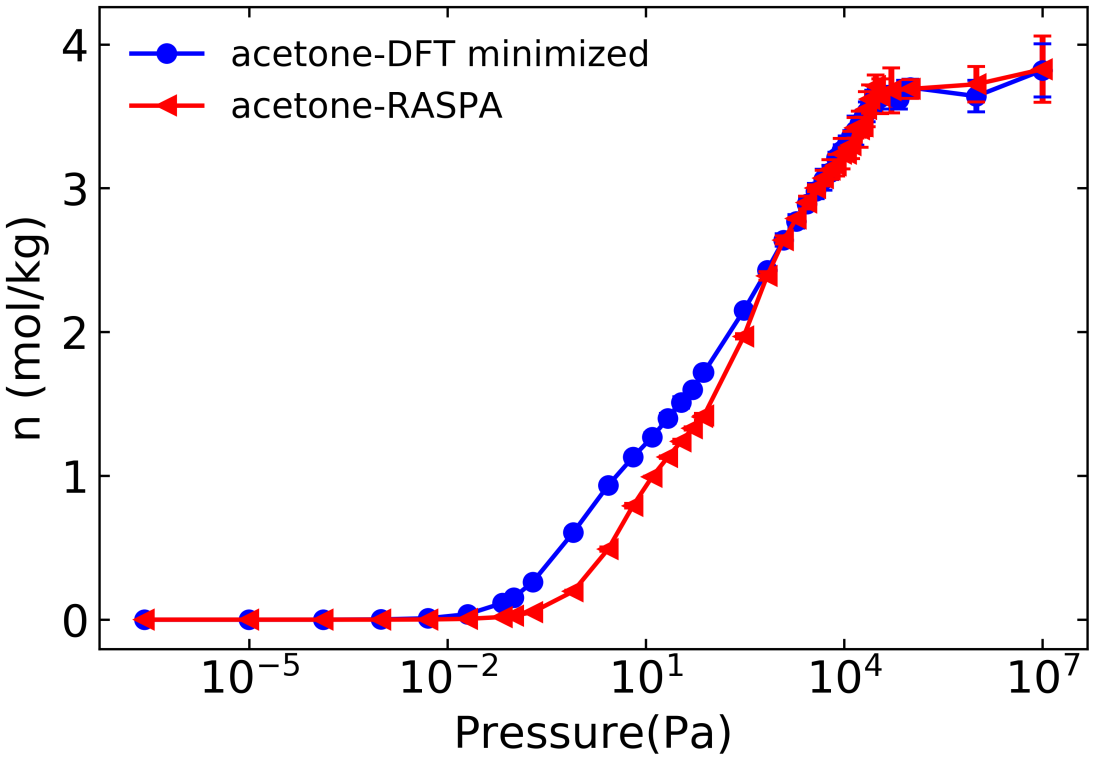

Figure 29: Adsorption isotherm of acetone at 298 K in LAMMPS DFT minimized structure and RASPA triclinic cell

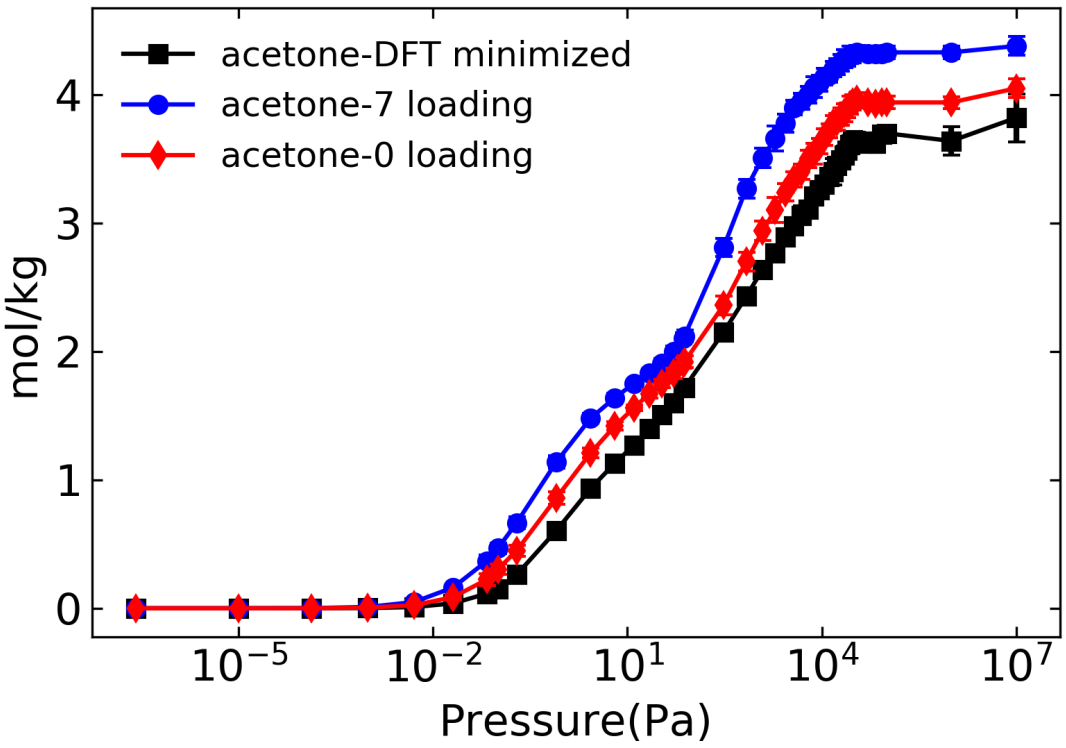

Figure 30: Adsorption isotherm of acetone at 298 K in DFT minimized structure, 7 loading of acetone UiO-66 and empty UiO-66 MD generated snapshots

Bibliography

[1] Hiroyasu Furukawa, Kyle E Cordova, Michael O'Keeffe, and Omar M Yaghi. The chemistry and applications of metal-organic frameworks. *Science*, 341(6149), 2013.

[2] Hong-Cai Zhou, Jeffrey R Long, and Omar M Yaghi. Introduction to metal–organic frameworks. *Chemical reviews*, 112(2):673–674, 2012.

[3] Jonathan P Ruffley, Isabella Goodenough, Tian-Yi Luo, Melissandre Richard, Eric Borguet, Nathaniel L Rosi, and J Karl Johnson. Design, synthesis, and characterization of metal–organic frameworks for enhanced sorption of chemical warfare agent simulants. *The Journal of Physical Chemistry C*, 123(32):19748–19758, 2019.

[4] Ayda Nemati Vesali Azar and Seda Keskin. Computational screening of mofs for acetylene separation. *Frontiers in chemistry*, 6:36, 2018.

[5] Lin Li, Sen Zhang, Jonathan P Ruffley, and J Karl Johnson. Energy efficient formaldehyde synthesis by direct hydrogenation of carbon monoxide in functionalized metal–organic frameworks. *ACS Sustainable Chemistry & Engineering*, 7(2):2508–2515, 2018.

[6] Sangil Han, Yougui Huang, Taku Watanabe, Sankar Nair, Krista S Walton, David S Sholl, and J Carson Meredith. Mof stability and gas adsorption as a function of exposure to water, humid air, so2, and no2. *Microporous and mesoporous materials*, 173:86–91, 2013.

[7] T Grant Glover, Gregory W Peterson, Bryan J Schindler, David Britt, and Omar Yaghi. Mof-74 building unit has a direct impact on toxic gas adsorption. *Chemical Engineering Science*, 66(2):163–170, 2011.

[8] Mohd Zamidi Ahmad, Thijs A Peters, Nora M Konnertz, Tymen Visser, Carlos Téllez, Joaquín Coronas, Vlastimil Fila, Wiebe M de Vos, and Nieck E Benes. High-pressure co2/ch4 separation of zr-mofs based mixed matrix membranes. *Separation and purification technology*, 230:115858, 2020.

[9] Tae-Hyun Bae, Jong Suk Lee, Wulin Qiu, William J Koros, Christopher W Jones, and Sankar Nair. A high-performance gas-separation membrane containing submicrometer-sized metal–organic framework crystals. *Angewandte Chemie*, 122(51):10059–10062, 2010.

[10] Mona H Mohamed, Yahui Yang, Lin Li, Sen Zhang, Jonathan P Ruffley, Austin Gamble Jarvi, Sunil Saxena, Götz Veser, J Karl Johnson, and Nathaniel L Rosi. Designing open metal sites in metal–organic frameworks for paraffin/olefin separations. *Journal of the American Chemical Society*, 141(33):13003–13007, 2019.

[11] Zhenzhen Xie, Tao Li, Nathaniel L Rosi, and Moises A Carreon. Alumina-supported cobalt–adeninate mof membranes for co 2/ch 4 separation. *Journal of Materials Chemistry A*, 2(5):1239–1241, 2014.

[12] Michael J Katz, Zachary J Brown, Yamil J Colón, Paul W Siu, Karl A Scheidt, Randall Q Snurr, Joseph T Hupp, and Omar K Farha. A facile synthesis of uio-66, uio-67 and their derivatives. *Chemical Communications*, 49(82):9449–9451, 2013.

[13] Jasmina Hafizovic Cavka, Søren Jakobsen, Unni Olsbye, Nathalie Guillou, Carlo Lamberti, Silvia Bordiga, and Karl Petter Lillerud. A new zirconium inorganic building brick forming metal organic frameworks with exceptional stability. *Journal of the American Chemical Society*, 130(42):13850–13851, 2008.

[14] M Kandiah, MH Nilsen, and S Usseglio. S. r. jakobsen, u. olsbye, m. tilset, c. larabi, ea quadrelli, f. bonino and kp lillerud. *Chem. Mater*, 22:6632–6640, 2010.

[15] Sergio J Garibay and Seth M Cohen. Isoreticular synthesis and modification of frameworks with the uio-66 topology. *Chemical Communications*, 46(41):7700–7702, 2010.

[16] William Morris, Christian J Doonan, and Omar M Yaghi. Postsynthetic modification of a metal–organic framework for stabilization of a hemiaminal and ammonia uptake. *Inorganic chemistry*, 50(15):6853–6855, 2011.

[17] Hai-Long Jiang, Dawei Feng, Tian-Fu Liu, Jian-Rong Li, and Hong-Cai Zhou. Pore surface engineering with controlled loadings of functional groups via click chemistry in highly stable metal–organic frameworks. *Journal of the American Chemical Society*, 134(36):14690–14693, 2012.

[18] Maw Lin Foo, Satoshi Horike, Tomohiro Fukushima, Yuh Hijikata, Yoshiki Kubota, Masaki Takata, and Susumu Kitagawa. Ligand-based solid solution approach to stabilisation of sulphonic acid groups in porous coordination polymer zr 6 o 4 (oh) 4 (bdc) 6 (uio-66). *Dalton transactions*, 41(45):13791–13794, 2012.

[19] V Guillerm, Florence Ragon, M Dan-Hardi, Thomas Devic, M Vishnuvarthan, B Campo, A Vimont, G Clet, Q Yang, G Maurin, et al. A series of isoreticular,

highly stable, porous zirconium oxide based metal–organic frameworks. *Angewandte Chemie*, 124(37):9401–9405, 2012.

[20] Qingyuan Yang, Hervé Jobic, Fabrice Salles, Daniil Kolokolov, Vincent Guillerm, Christian Serre, and Guillaume Maurin. Probing the dynamics of co2 and ch4 within the porous zirconium terephthalate uio-66 (zr): A synergic combination of neutron scattering measurements and molecular simulations. *Chemistry–A European Journal*, 17(32):8882–8889, 2011.

[21] Min Kim, John F Cahill, Honghan Fei, Kimberley A Prather, and Seth M Cohen. Postsynthetic ligand and cation exchange in robust metal–organic frameworks. *Journal of the American Chemical Society*, 134(43):18082–18088, 2012.

[22] Hui Wu, Taner Yildirim, and Wei Zhou. Exceptional mechanical stability of highly porous zirconium metal–organic framework uio-66 and its important implications. *The journal of physical chemistry letters*, 4(6):925–930, 2013.

[23] Kent O Kirlikovali, Zhijie Chen, Timur Islamoglu, Joseph T Hupp, and Omar K Farha. Zirconium-based metal–organic frameworks for the catalytic hydrolysis of organophosphorus nerve agents. *ACS applied materials & interfaces*, 12(13):14702–14720, 2020.

[24] Yangyang Liu, Ashlee J Howarth, Nicholaas A Vermeulen, Su-Young Moon, Joseph T Hupp, and Omar K Farha. Catalytic degradation of chemical warfare agents and their simulants by metal-organic frameworks. *Coordination Chemistry Reviews*, 346:101–111, 2017.

[25] Joseph E Mondloch, Michael J Katz, William C Isley Iii, Pritha Ghosh, Peilin Liao, Wojciech Bury, George W Wagner, Morgan G Hall, Jared B DeCoste, Gregory W Peterson, et al. Destruction of chemical warfare agents using metal–organic frameworks. *Nature materials*, 14(5):512–516, 2015.

[26] Timur Islamoglu, Zhijie Chen, Megan C Wasson, Cassandra T Buru, Kent O Kirlikovali, Unjila Afrin, Mohammad Rasel Mian, and Omar K Farha. Metal–organic frameworks against toxic chemicals. *Chemical reviews*, 120(16):8130–8160, 2020.

[27] Florencia A Son, Megan C Wasson, Timur Islamoglu, Zhijie Chen, Xinyi Gong, Sylvia L Hanna, Jiafei Lyu, Xingjie Wang, Karam B Idrees, John J Mahle, et al. Uncovering the role of metal–organic framework topology on the capture and reactivity of chemical warfare agents. *Chemistry of Materials*, 32(11):4609–4617, 2020.

[28] Yi Feng, Qian Chen, Minqi Jiang, and Jianfeng Yao. Tailoring the properties of uio-66 through defect engineering: a review. *Industrial & Engineering Chemistry Research*, 58(38):17646–17659, 2019.

[29] Yan Bai, Yibo Dou, Lin-Hua Xie, William Rutledge, Jian-Rong Li, and Hong-Cai Zhou. Zr-based metal–organic frameworks: design, synthesis, structure, and applications. *Chemical Society Reviews*, 45(8):2327–2367, 2016.

[30] Zubair Hasan, Nazmul Abedin Khan, and Sung Hwa Jhung. Adsorptive removal of diclofenac sodium from water with zr-based metal–organic frameworks. *Chemical Engineering Journal*, 284:1406–1413, 2016.

[31] Andreas Schaate, Pascal Roy, Adelheid Godt, Jann Lippke, Florian Waltz, Michael Wiebcke, and Peter Behrens. Modulated synthesis of zr-based metal–organic frameworks: from nano to single crystals. *Chemistry–A European Journal*, 17(24):6643–6651, 2011.

[32] Loredana Valenzano, Bartolomeo Civalleri, Sachin Chavan, Silvia Bordiga, Merete H Nilsen, Søren Jakobsen, Karl Petter Lillerud, and Carlo Lamberti. Disclosing the complex structure of uio-66 metal organic framework: a synergic combination of experiment and theory. *Chemistry of Materials*, 23(7):1700–1718, 2011.

[33] Greig C Shearer, Stian Forselv, Sachin Chavan, Silvia Bordiga, Karina Mathisen, Morten Bjørgen, Stian Svelle, and Karl Petter Lillerud. In situ infrared spectroscopic and gravimetric characterisation of the solvent removal and dehydroxylation of the metal organic frameworks uio-66 and uio-67. *Topics in Catalysis*, 56(9-10):770–782, 2013.

[34] Mayank Agrawal, Salah E Boulfelfel, Dorina F Sava Gallis, Jeffery A Greathouse, and David S Sholl. Determining diffusion coefficients of chemical warfare agents in metal–organic frameworks. *The journal of physical chemistry letters*, 10(24):7823–7830, 2019.

[35] Hui Wu, Yong Shen Chua, Vaiva Krungleviciute, Madhusudan Tyagi, Ping Chen, Taner Yildirim, and Wei Zhou. Unusual and highly tunable missing-linker defects in zirconium metal–organic framework uio-66 and their important effects on gas adsorption. *Journal of the American Chemical Society*, 135(28):10525–10532, 2013.

[36] Bart Bueken, Niels Van Velthoven, Andraž Krajnc, Simon Smolders, Francis Taulelle, Caroline Mellot-Draznieks, Gregor Mali, Thomas D Bennett, and Dirk De Vos. Tack-

ling the defect conundrum in uio-66: a mixed-linker approach to engineering missing linker defects. *Chemistry of Materials*, 29(24):10478–10486, 2017.

[37] Bing Li, Xiangyang Zhu, Kaili Hu, Yongsheng Li, Jianfang Feng, Jianlin Shi, and Jinlou Gu. Defect creation in metal-organic frameworks for rapid and controllable decontamination of roxarsone from aqueous solution. *Journal of hazardous materials*, 302:57–64, 2016.

[38] Xiao Liu, Wei Qi, Yuefei Wang, Rongxin Su, and Zhimin He. A facile strategy for enzyme immobilization with highly stable hierarchically porous metal–organic frameworks. *Nanoscale*, 9(44):17561–17570, 2017.

[39] Wenlong Xu, Kedar Bahadur Thapa, Qiang Ju, Zhenlan Fang, and Wei Huang. Heterogeneous catalysts based on mesoporous metal–organic frameworks. *Coordination Chemistry Reviews*, 373:199–232, 2018.

[40] Keke Wang, Caifeng Li, Yuxin Liang, Tongtong Han, Hongliang Huang, Qingyuan Yang, Dahuan Liu, and Chongli Zhong. Rational construction of defects in a metal–organic framework for highly efficient adsorption and separation of dyes. *Chemical Engineering Journal*, 289:486–493, 2016.

[41] David S Sholl and Ryan P Lively. Defects in metal–organic frameworks: challenge or opportunity? *The journal of physical chemistry letters*, 6(17):3437–3444, 2015.

[42] Pritha Ghosh, Yamil J Colón, and Randall Q Snurr. Water adsorption in uio-66: the importance of defects. *Chemical communications*, 50(77):11329–11331, 2014.

[43] Yang Jiao, Yang Liu, Guanghui Zhu, Julian T Hungerford, Souryadeep Bhattacharyya, Ryan P Lively, David S Sholl, and Krista S Walton. Heat-treatment of defective uio-66 from modulated synthesis: Adsorption and stability studies. *The Journal of Physical Chemistry C*, 121(42):23471–23479, 2017.

[44] Xiaodong Zhang, Yang Yang, Liang Song, Jinfeng Chen, Yiqiong Yang, and Yuxin Wang. Enhanced adsorption performance of gaseous toluene on defective uio-66 metal organic framework: equilibrium and kinetic studies. *Journal of hazardous materials*, 365:597–605, 2019.

[45] Liyong Yuan, Ming Tian, Jianhui Lan, Xingzhong Cao, Xiaolin Wang, Zhifang Chai, John K Gibson, and Weiqun Shi. Defect engineering in metal–organic frameworks:

a new strategy to develop applicable actinide sorbents. *Chemical Communications*, 54(4):370–373, 2018.

[46] Greig C Shearer, Sachin Chavan, Silvia Bordiga, Stian Svelle, Unni Olsbye, and Karl Petter Lillerud. Defect engineering: tuning the porosity and composition of the metal–organic framework uio-66 via modulated synthesis. *Chemistry of Materials*, 28(11):3749–3761, 2016.

[47] Jessica K Bristow, Katrine L Svane, Davide Tiana, Jonathan M Skelton, Julian D Gale, and Aron Walsh. Free energy of ligand removal in the metal–organic framework uio-66. *The Journal of Physical Chemistry C*, 120(17):9276–9281, 2016.

[48] David Dubbeldam, Sofía Calero, Donald E Ellis, and Randall Q Snurr. Raspa: molecular simulation software for adsorption and diffusion in flexible nanoporous materials. *Molecular Simulation*, 42(2):81–101, 2016.

[49] Mayank Agrawal, Dorina F Sava Gallis, Jeffery A Greathouse, and David S Sholl. How useful are common simulants of chemical warfare agents at predicting adsorption behavior? *The Journal of Physical Chemistry C*, 122(45):26061–26069, 2018.

[50] Michael P Allen and Dominic J Tildesley. *Computer simulation of liquids*. Oxford university press, 2017.

[51] Paul P Ewald. Die berechnung optischer und elektrostatischer gitterpotentiale. *Annalen der physik*, 369(3):253–287, 1921.

[52] Thomas A Manz and Nidia Gabaldon Limas. Introducing ddec6 atomic population analysis: part 1. charge partitioning theory and methodology. *RSC advances*, 6(53):47771–47801, 2016.

[53] Nidia Gabaldon Limas and Thomas A Manz. Introducing ddec6 atomic population analysis: part 2. computed results for a wide range of periodic and nonperiodic materials. *RSC advances*, 6(51):45727–45747, 2016.

[54] Thomas A Manz. Introducing ddec6 atomic population analysis: part 3. comprehensive method to compute bond orders. *RSC advances*, 7(72):45552–45581, 2017.

[55] Nidia Gabaldon Limas and Thomas A Manz. Introducing ddec6 atomic population analysis: part 4. efficient parallel computation of net atomic charges, atomic spin moments, bond orders, and more. *RSC advances*, 8(5):2678–2707, 2018.

[56] Anthony K Rappé, Carla J Casewit, KS Colwell, William A Goddard III, and W Mason Skiff. Uff, a full periodic table force field for molecular mechanics and molecular dynamics simulations. *Journal of the American chemical society*, 114(25):10024–10035, 1992.

[57] Stephen L Mayo, Barry D Olafson, and William A Goddard. Dreiding: a generic force field for molecular simulations. *Journal of Physical chemistry*, 94(26):8897–8909, 1990.

[58] Greig C Shearer, Sachin Chavan, Jayashree Ethiraj, Jenny G Vitillo, Stian Svelle, Unni Olsbye, Carlo Lamberti, Silvia Bordiga, and Karl Petter Lillerud. Tuned to perfection: ironing out the defects in metal–organic framework uio-66. *Chemistry of Materials*, 26(14):4068–4071, 2014.

[59] Bin Chen, Jeffrey J Potoff, and J Ilja Siepmann. Monte carlo calculations for alcohols and their mixtures with alkanes. transferable potentials for phase equilibria. 5. united-atom description of primary, secondary, and tertiary alcohols. *The Journal of Physical Chemistry B*, 105(15):3093–3104, 2001.

[60] Ronen Zangi. Refinement of the oplsaa force-field for liquid alcohols. *ACS omega*, 3(12):18089–18099, 2018.

[61] Jacob J Wardzala, Jonathan P Ruffley, Isabella Goodenough, Allie M Schmidt, Priyanka B Shukla, Xin Wei, Abhishek Bagusetty, Mattheus De Souza, Prasenjit Das, Dorian J Thompson, et al. Modeling of diffusion of acetone in uio-66. *The Journal of Physical Chemistry C*, 2020.

[62] John M Stubbs, Jeffrey J Potoff, and J Ilja Siepmann. Transferable potentials for phase equilibria. 6. united-atom description for ethers, glycols, ketones, and aldehydes. *The Journal of Physical Chemistry B*, 108(45):17596–17605, 2004.

[63] Jongwoo Park, Ryan P Lively, and David S Sholl. Establishing upper bounds on co 2 swing capacity in sub-ambient pressure swing adsorption via molecular simulation of metal–organic frameworks. *Journal of Materials Chemistry A*, 5(24):12258–12265, 2017.

[64] Jongwoo Park, Joshua D Howe, and David S Sholl. How reproducible are isotherm measurements in metal–organic frameworks? *Chemistry of Materials*, 29(24):10487–10495, 2017.

[65] Dai Tang, Ying Wu, Ross J Verploegh, and David S Sholl. Efficiently exploring adsorption space to identify privileged adsorbents for chemical separations of a diverse set of molecules. *ChemSusChem*, 11(9):1567–1575, 2018.

[66] Seda Keskin and David S Sholl. Screening metal- organic framework materials for membrane-based methane/carbon dioxide separations. *The Journal of Physical Chemistry C*, 111(38):14055–14059, 2007.

[67] Cigdem Altintas, Gokay Avci, Hilal Daglar, Ayda Nemati Vesali Azar, Sadiye Velioglu, Ilknur Erucar, and Seda Keskin. Database for co2 separation performances of mofs based on computational materials screening. *ACS applied materials & interfaces*, 10(20):17257–17268, 2018.

[68] Tina Düren, Youn-Sang Bae, and Randall Q Snurr. Using molecular simulation to characterise metal–organic frameworks for adsorption applications. *Chemical Society Reviews*, 38(5):1237–1247, 2009.

[69] François-Xavier Coudert and Alain H Fuchs. Computational characterization and prediction of metal–organic framework properties. *Coordination Chemistry Reviews*, 307:211–236, 2016.

[70] JR Li. Y. 105 ma, mc mccarthy, j. sculley, j. yu, hk jeong, pb balbuena and hc zhou. *Coord. Chem. Rev*, 255:1791–1823, 2011.

[71] Seda Keskin, Jinchen Liu, Rees B Rankin, J Karl Johnson, and David S Sholl. Progress, opportunities, and challenges for applying atomically detailed modeling to molecular adsorption and transport in metal- organic framework materials. *Industrial & Engineering Chemistry Research*, 48(5):2355–2371, 2009.

[72] Gérard Férey and Christian Serre. Large breathing effects in three-dimensional porous hybrid matter: facts, analyses, rules and consequences. *Chemical Society Reviews*, 38(5):1380–1399, 2009.

[73] Jae Hwa Lee, Sungeun Jeoung, Yongchul G Chung, and Hoi Ri Moon. Elucidation of flexible metal-organic frameworks: Research progresses and recent developments. *Coordination Chemistry Reviews*, 389:161–188, 2019.

[74] Brian R Pimentel, Melinda L Jue, Er-Kang Zhou, Ross J Verploegh, Johannes Leisen, David S Sholl, and Ryan P Lively. Sorption and transport of vapors in zif-11:

adsorption, diffusion, and linker flexibility. *The Journal of Physical Chemistry C*, 123(20):12862–12870, 2019.

[75] Andrzej Gładysiak, Kathryn S Deeg, Iurii Dovgaliuk, Arunraj Chidambaram, Kaili Ordiz, Peter G Boyd, Seyed Mohamad Moosavi, Daniele Ongari, Jorge AR Navarro, Berend Smit, et al. Biporous metal–organic framework with tunable co2/ch4 separation performance facilitated by intrinsic flexibility. *ACS applied materials & interfaces*, 10(42):36144–36156, 2018.

[76] Jongwoo Park, Mayank Agrawal, Dorina F Sava Gallis, Jacob A Harvey, Jeffery A Greathouse, and David S Sholl. Impact of intrinsic framework flexibility for selective adsorption of sarin in non-aqueous solvents using metal–organic frameworks. *Physical Chemistry Chemical Physics*, 22(11):6441–6448, 2020.

[77] Matthew Witman, Sanliang Ling, Sudi Jawahery, Peter G Boyd, Maciej Haranczyk, Ben Slater, and Berend Smit. The influence of intrinsic framework flexibility on adsorption in nanoporous materials. *Journal of the American Chemical Society*, 139(15):5547–5557, 2017.

[78] Matthew Witman, Bradley Wright, and Berend Smit. Simulating enhanced methane deliverable capacity of guest responsive pores in intrinsically flexible mofs. *The journal of physical chemistry letters*, 10(19):5929–5934, 2019.

[79] Jason A Gee and David S Sholl. Effect of framework flexibility on c8 aromatic adsorption at high loadings in metal–organic frameworks. *The Journal of Physical Chemistry C*, 120(1):370–376, 2016.

[80] Mayank Agrawal and David S Sholl. Effects of intrinsic flexibility on adsorption properties of metal–organic frameworks at dilute and nondilute loadings. *ACS applied materials & interfaces*, 11(34):31060–31068, 2019.

[81] Damien E Coupry, Matthew A Addicoat, and Thomas Heine. Extension of the universal force field for metal–organic frameworks. *Journal of Chemical Theory and Computation*, 12(10):5215–5225, 2016.

[82] Steve Plimpton. Fast parallel algorithms for short-range molecular dynamics. *Journal of computational physics*, 117(1):1–19, 1995.

[83] Sven MJ Rogge, Jelle Wieme, Louis Vanduyfhuys, Steven Vandenbrande, Guillaume Maurin, Toon Verstraelen, Michel Waroquier, and Veronique Van Speybroeck. Ther-

modynamic insight in the high-pressure behavior of uio-66: effect of linker defects and linker expansion. *Chemistry of Materials*, 28(16):5721–5732, 2016.

[84] Shuichi Nosé. A unified formulation of the constant temperature molecular dynamics methods. *The Journal of chemical physics*, 81(1):511–519, 1984.

[85] William G Hoover. Canonical dynamics: Equilibrium phase-space distributions. *Physical review A*, 31(3):1695, 1985.

[86] Taku Watanabe and David S Sholl. Accelerating applications of metal–organic frameworks for gas adsorption and separation by computational screening of materials. *Langmuir*, 28(40):14114–14128, 2012.

[87] Emmanuel Haldoupis, Taku Watanabe, Sankar Nair, and David S Sholl. Quantifying large effects of framework flexibility on diffusion in mofs: Ch4 and co2 in zif-8. *ChemPhysChem*, 13(15):3449–3452, 2012.